ACS OMEGA

Open Access

http://pubs.acs.org/journal/acsodf

Article

Discovery of Novel Multiangiogenic Agents Targeting VEGFR2, EphB4, FGFR-1, and TIE-2: Receptor-Based Pharmacophore Modeling, Virtual Screening, and Molecular Modeling Studies

Jeevan Patra, Amit K. Keshari,* Richie R. Bhandare,* Afzal B. Shaik, Madison Parrot, and Shiru Lin

Cite This: *ACS Omega* 2025, 10, 13880−13897

Read Online

ACCESS | Metrics & More | Article Recommendations | Supporting Information

ABSTRACT: The angiogenesis phenomenon is crucial for the formation of new blood vessels in cancer cells. The cancerous cells' progress hampers other healthy cells. The main objective of this study is to explore and decipher multimodal natural compounds against VEGFR2, EphB4, FGFR-1, and TIE-2 drug targets to arrest angiogenesis and progression. The receptor-based pharmacophore modeling of VEGFR2, EphB4, FGFR-1, and TIE-2 was developed and validated through enrichment parameters. Further, the validated hypothesis allowed for screening druglike natural product databases such as SuperNatural 3.0, COCONUT, and LOTUS. The common pharmacophoric featured natural compounds were assessed for binding affinities using absolute end-point methods. Finally, density functional theory has been studied to understand the chemical reactivity and stability of the protein complexes. Among all of the screened natural compounds, 17 natural compounds were found to align accurately against validated pharmacophore models having higher fitness scores and align scores. Taking reference drugs sorafenib (VEGFR2), NVP-BHG712 (EphB4), pemiganitib (FGFR-1), and DP1919 (TIE-2), three promising natural compounds CNP0003920, CNP0243075, and CNP0211397 were concluded based on their end-point binding energies, binding interactions, molecular dynamics, and optimal pharmacokinetic and toxicity profiles. The density functional theory (DFT) results suggested that the identified compounds bound with protein complexes are stable. Our findings can represent a promising starting point for developing multimodal analogues VEGFR2, EphB4, FGFR-1, and TIE-2 proteins.

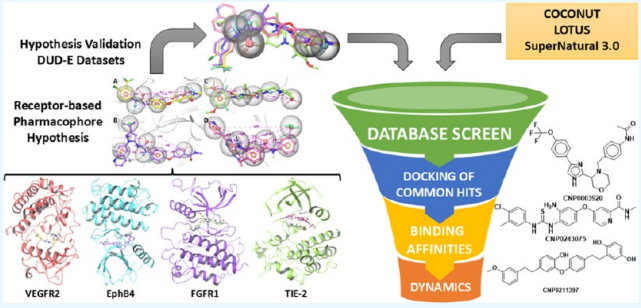

1. INTRODUCTION

Angiogenesis, the formation of new blood vessels from existing ones, is a complex and dynamic process regulated by various pro- and antiangiogenic molecules.[1,2] It plays a crucial role in tumor growth, invasion, and metastasis, making it an attractive target for cancer therapy.[1,3] Over the past decades, significant progress has been made in understanding the molecular mechanisms underlying tumor angiogenesis and developing antiangiogenic therapies. One of the most widely studied targets for antiangiogenic therapy is the vascular endothelial growth factor (VEGFR) pathway, which promotes endothelial cell survival, proliferation, and migration.[4] VEGFR families mainly consist of VEGFR-1, VEGFR2, and VEGFR-3. Among all VEGFR families, VEGFR2 plays an essential role in tumor angiogenesis in endothelial cells,[5−7] and due to overexpression, myriads of cancers are being developed.[8−10] Studies suggested that the erythropoietin-producing hepatocyte receptor B4 (EphB4) and its transmembrane-type ligand (ephrin B2) are crucial for angiogenesis, vessel maturation, and pericyte recruitment.[11−14] The angiopoietin (TIE-2) and EphB4 proteins are essential for vessel stabilization,[15] maturation, remodeling of vasculature, vascular development,[16] and prognosis.[17] The human FGFR comprises four isoforms that are expressed on the cell membrane and have vital physiological and pathological processes, such as proliferation, differentiation, cell migration, survival, and angiogenesis.[18] Among all four isoforms, FGFR-1 is overexpressed and amplified in various cancers.[19] Hence, it is believed that the development of small molecules competitively binding at the ATP binding site of FGFR-1 presents a promising approach for cancer treatment. Several monoclonal antibodies such as bevacizumab, ranibizumab, and pegaptanib and receptor tyrosine kinase inhibitors (RTKs) targeting VEGFRs such as sunitinib, sorafenib, regorafenib, and pazopanib have been clinically approved for the treatment of various carcinomas.[20−23] Despite having promising efficacy, their clinical benefits are still limited due to the presence of adverse events, acquired drug resistance, and tumor recurrence. For example, bevacizumab antibody causes severe eye inflammation,[24] while

Received: September 11, 2024
Revised: January 20, 2025
Accepted: January 27, 2025
Published: April 1, 2025

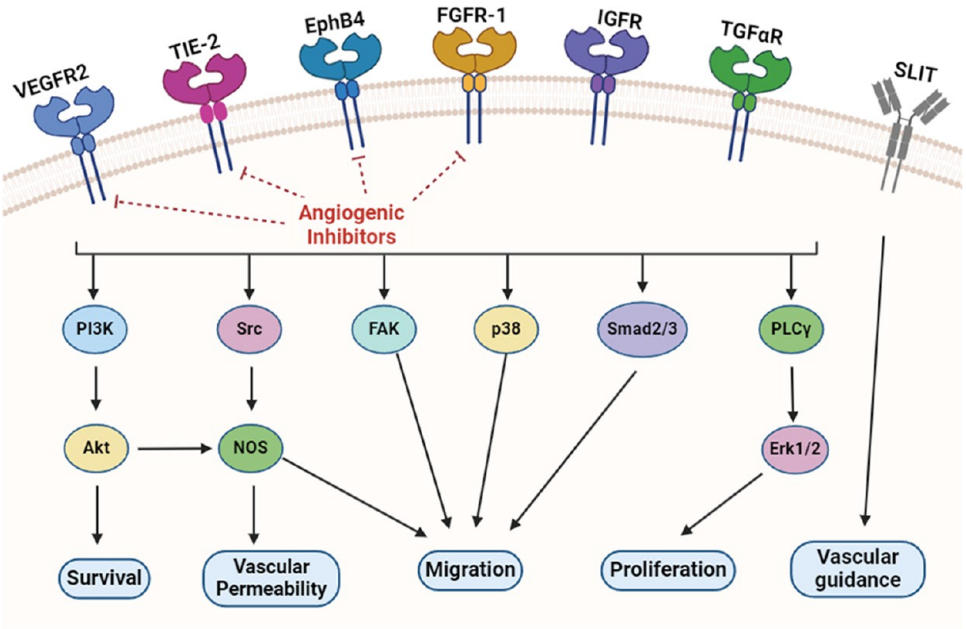

Figure 1. Rationale design strategy and potential mechanisms of multitarget anti-angiogenic agents targeting VEGFR2, EphB4, FGFR-1, and TIE-2.

sunitinib causes thrombocytopenia and hypertension.[25] These challenges are conferred by targeting a single angiogenic pathway. A few mounting evidences revealed that tumors become refractory and bypass via a single pro-angiogenic factor via compensatory activation of alternative pro-angiogenic factors.[26] Therefore, to address this multicompensatory activation profile simultaneous inhibition and combinatorial targeting of multiple pro-angiogenic RTKs is utmost essential. Thus, in this present study, we undertook to identify inhibitors that could be capable of having broader inhibition, targeting critical sites in angiogenesis pathways. Many studies have been reported showing multitargeted potent activity against these targets. In recent years, multimodal agents have been performed and validated using computational and biochemical assays.[27−32]

Natural products could be attractive chemotypes for addressing the challenges above due to their plethora of benefits such as structural diversity,[33] broader pharmacological bioactivity, lesser toxicity,[34] and minimal drug resistance[35] over the synthetic drugs. Hence, natural products serve as the pivotal source for the development of new regimens in ethnopharmacological research.[36] Previously, a natural alkaloid taspine conjugated with salicylaldoxime had been designed and validated for its potency toward triple VEGFR2/TIE-2/EphB4 as antiangiogenic.[37] This multitargeted antiangiogenic agent offered possibility due to the structural similarity and globally conserved region conformations of the VEGFR2, TIE-2, and EphB4 proteins.[38] In the RTKs structure, the highly conserved aspartate-phenylalanine-glycine (DFG motif) triad represented as an activation loop is essential for kinase activity,[39] conserved catalytic site binding with ATP, and ATP binding sites are quite identical.

In this study, natural product databases are considered for high-throughput virtual screening. The inclusion of NP-like chemotypes alongside natural product databases in our screening approach provides several strategic advantages in drug discovery. NP-like compounds maintain beneficial structural features and biological relevance while offering improved synthetic accessibility and optimization potential over natural products with complex structures.[40−43] These compounds effectively explore the adjacent chemical space while retaining privileged scaffolds and pharmacophoric elements of natural products, thereby filling crucial gaps in the natural product chemical space.[44] Furthermore, NP-like compounds can be designed to better align with druglike property requirements while preserving the characteristic biological activity patterns of natural products.[45,46] The biology-oriented synthesis approach further supports the rationale for including NP-like compounds in virtual screening campaigns.[47] They complement NP databases by providing additional chemical diversity while maintaining biological relevance. This comprehensive screening strategy enhances our ability to identify potential NP-likeness multiangiogenic inhibitors with favorable clinical-like candidates.

Structure-based virtual screening has been a benchmark in the early-stage drug discovery paradigm. Several approaches have been utilized, such as receptor-guided drug design, ligand-based drug design, pharmacophore modeling, and similarity chemical space explorations for the identification of potential lead drugs. Pharmacophore modeling has been versatile due to its conformational and developed hypothesis features explored from the databases, which ease in screening the chemical space.[48] Virtual screening allows us to explore a vast chemical space to acquire for biological evaluations. Utilizing multiple parameters for screening virtual libraries embedded with augmented molecular modeling became a holistic approach for the identification of lead hits in early-stage drug discovery.[49,50]

Encouraged by the above facts, in the present study, we pioneered and unveiled the potential of NP-like chemotypes against VEGFR2, EphB4, FGFR-1, and TIE-2 proteins (Figure 1). These are achieved by developing an energy-based pharmacophore model using cocrystallized type-II RTK inhibitors. Initially, the generated pharmacophore models are utilized to screen virtually with natural databases tailored with diverse scaffolds to satisfy high fold alignment. Further, the commonly featured natural compounds were estimated for their molecular binding behavior and binding free energies

https://doi.org/10.1021/acsomega.4c08366
ACS Omega 2025, 10, 13880−13897

using end-point methods. Finally, the best-identified hits were assessed for stability analysis using molecular dynamics simulations.

2. COMPUTATIONAL METHODOLOGIES

2.1. Structural Crystallography Preparations. The crystallography structures of VEGFR2 (PDB ID: 4ASD),[51] EphB4 (PDB ID: 6FNI),[52] FGFR-1 (PDB ID: 7WCL),[53] and TIE-2 (PDB ID: 6MWE)[54] cocrystallized with type-II inhibitors were obtained from the RCSB PDB bank. For all crystallography, only chain A was considered, and other chains were removed. The crystallographic species such as heteroatoms, cofactors, and solvents were removed. The proteins were analyzed to fill any missing loops and side chains using Prime. The proteins were protonated at pH 7.0 ± 2.0 using PROPKA. Further, the hydrogens were assigned, optimized, and minimized until the system reached a RMSD less than 0.3 Å using the OPLS-4 force field.

2.2. Protein Sequence Alignment. The FASTA sequences of all proteins were subjected to the MUSCLE program[55] to align and visualize the sequence similarity. VEGFR2 is used as an input query template, and EphB4, FGFR-1, and TIE-2 are used as input subject templates.

2.3. Virtual Database Curation and Preparations. The database construction was performed based on the designed workflow (Figure 2). In the current study, a virtual database

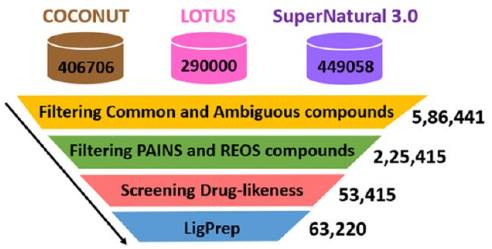

Figure 2. Flowchart of virtual database preparations.

was constructed from COCONUT (COlleCtion of Open Natural ProdUcTs),[56] LOTUS,[57] and SuperNatural 3.0[58] comprising 406,706, 290,000, and 449,058 natural compounds, respectively. The common natural compounds, ambiguous structures, and broken fragments were filtered by using the RDKit program. The unique natural compounds (5,86,441) were screened for pan assay interferences (PAINS) and rapid elimination of swill (REOS) using False Positive Remover.[59] Further, these filtered natural compounds (2,25,415) were computed using the QikProp module to assess drug-likeness (without Lipinski's rule of five violations). From this stage, only 53,415 natural compounds were preprocessed using the LigPrep module. All possible ionizable states as well as tautomeric forms in the pH range of 7.0 ± 2.0 were generated using the Epik function of LigPrep. For each ligand, at most 32 conformers were generated by default, and low-energy stereoisomers with correct chirality were engaged for further study. The final virtual database is composed of 63,220 natural compounds.

2.4. Development of Pharmacophore Hypothesis and Validation. The e-pharmacophore function of the phase module was used to develop the pharmacophore hypothesis of all structural complexes.[60,61] The chemical attributes such as the hydrogen bond donor (HBD), hydrogen bond acceptor (HBA), hydrophobic group (H), positive (P) and negative (N) ionizable groups, and aromatic ring (R) were used to generate e-pharmacophore sites. For validation, the active and decoy sets of VEGFR2, EphB4, FGFR-1, and TIE-2 were retrieved from DEKOIS 2.0 (demanding evaluation kits for objective *in silico* screening) and Directory of Useful Decoys: Enhanced (DUD-E) databases. These databases were prepared by using default parameters present in the LigPrep module. The validation of designed e-pharmacophore models is a crucial step to validate accuracy and specificity in selecting active reliable ligands using high-throughput screening from a virtual database. The statistical parameters such as the enrichment factor (EF), robust initial enhancement (RIE), Boltzmann-enhanced discrimination of receiver operating characteristic (BEDROC), accumulation curve (AUAC), and receiving operating curve (ROC) were estimated based on the respective active and decoy data sets.[62]

2.5. E-Pharmacophore-Based Database Screening. The validated pharmacophore hypothesis models were subjected to the natural product database screening (63,220 compounds) using default parameters of the phase module (Figure 3). For the screening of natural compounds, initially,

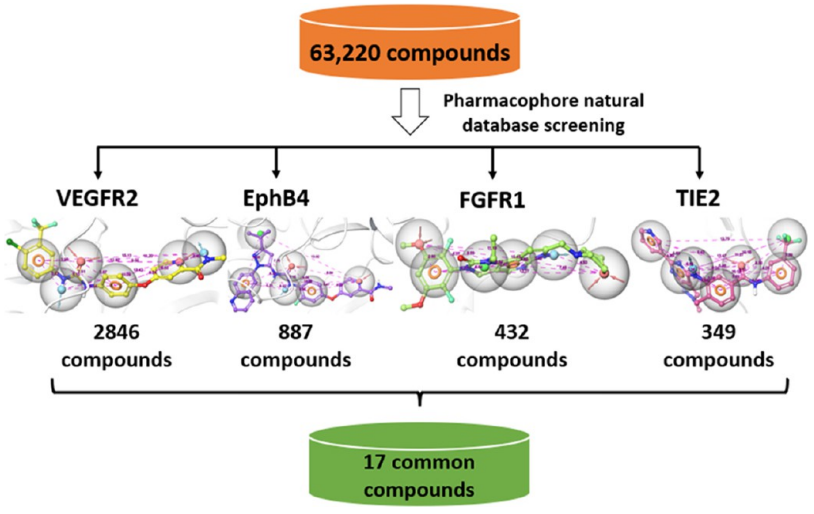

Figure 3. Workflow of phase screening for exploring common natural compounds.

https://doi.org/10.1021/acsomega.4c08366
ACS Omega 2025, 10, 13880−13897

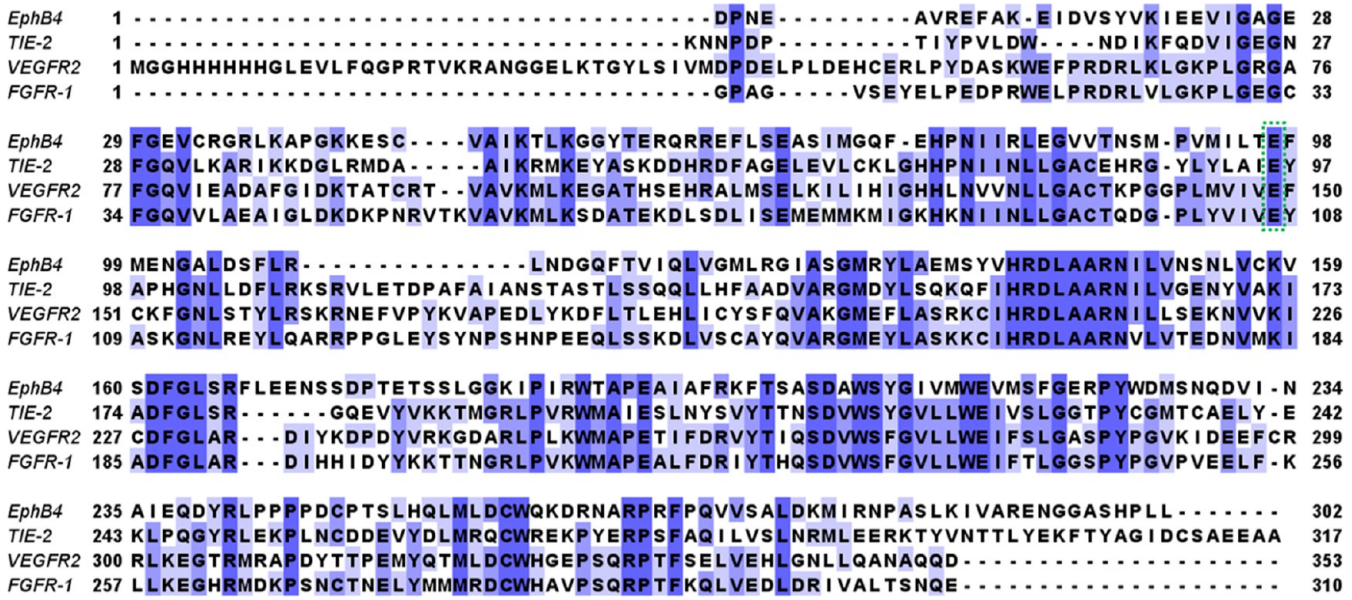

Figure 4. Multiple sequence alignment of four receptor tyrosine kinases showing identical patterns highlighted in blue color.

these were screened against all validated pharmacophore hypothesis models. The screening was performed based on the ligand matching at the conserved features (HBA, HBD, hydrophobic, aromatic) and multiple quantitative parameters such as the fitness score, align score, volume score, phase screen score, and vector score. The database-screened compounds against VEGFR2, EphB4, FGFR-1, and TIE-2 yielded 2846, 887, 432, and 349, respectively. The commonly screened natural compounds against all e-pharmacophore models were clustered based on the fitness/phase screen score having a cutoff >0.1. These final common compounds are composed of 17 compounds, which are used for binding affinity studies.

2.6. Receptor Grid Generation. The receptor grid of all proteins was generated using the receptor grid generation function embedded in the Glide module. The grid detects the cocrystallized ligands, which are centered to generate a three-dimensional (3D) box that is represented as the active binding site of the receptor. The gatekeeper, hinge loop, and DFG motif residues were allowed to form rotatable bonds for the formation of suitable interactions. The partial charge cutoff and scaling factor were kept at 0.25 and 1.0, respectively.

2.7. Molecular Docking and Binding Free Energy Estimation. The common 17 phase-screened natural compounds were fed for the virtual screening with Glide XP under the default parameters. For each ligand, three poses were generated and the best-scoring states were considered for postdocking analysis. The binding free energy was calculated using the molecular mechanics generalized Born surface area (MM-GBSA) method using the Prime module using default parameters. The best-docked poses were minimized utilizing the local optimization characteristics of Prime, and the energies of the complexes were calculated using a generalized Born/surface area (GB/SA) continuous solvent model under the OPLS-4 force field. The MM-GBSA of docked complexes was calculated using the equations:[63]

$$\Delta G_{\text{bind}} = \Delta E_{\text{MM}} + \Delta G_{\text{solv}} + \Delta G_{\text{SA}}$$

$$\Delta E_{\text{bind}} = E_{\text{complex}} - E_{\text{protein}} - E_{\text{ligand}}$$

where ΔE_{MM} is the difference between the minimized energies of the protein complexes and the sum of the minimized energies of unliganded proteins with its inhibitor, ΔG_{solv} is the difference between GBSA solvation energies of complexes and the sum of the GBSA solvation energies of the unliganded protein and inhibitor, and ΔG_{SA} is the difference between surface area energies of the complex and the sum of the surface area of the unliganded enzyme bound with its inhibitor.

2.8. Molecular Dynamics Simulations. Molecular dynamics (MD) simulation of protein−ligand complexes was performed by Desmond to expound changes in the conformation and stability of protein−ligand complexes through multiple trajectories. First, the best-docked conformer of protein−ligand complexes was introduced into Desmond. All complexes were built using a system builder with a TIP5P solvation model and neutralized using physiological salts at a 0.15 M concentration. Further, the systems were truncated in a cubic box of 10 Å in each direction. Through the steepest descent and limited memory of the Broyden−Fletcher−Goldfarb−Shanno (BFGS) algorithm, the system energy was reduced until reaching the gradient threshold of 25 kcal/mol/Å. The system was relaxed at a temperature and pressure of 300 K and 1.01325 bar, respectively. The MD simulations were performed for 100 ns for each 12 complexes in triplicates under the NPT system, in which the trajectory was recorded every 4.8 ps under the OPLS-4 force field.

2.9. Density Functional Theory. Density functional theory (DFT) is used to determine and validate enzymatic reaction mechanisms at the active binding sites. Electronic effects of druglike candidates are highly essential for the pharmacological effects. In this study, DFT was computed using Gaussian of the best potent hits using Becke's three-parameter exchange potential and the Lee−Yang−Parr correlation functional (B3LYP) theory with 6-31G* as the basis set.[64] The frontier molecular orbital (FMO) and molecular electrostatic potential (MESP) were computed between the highest occupied molecular orbital (HOMO) and the lowest unoccupied molecular orbital (LUMO).

https://doi.org/10.1021/acsomega.4c08366
ACS Omega 2025, 10, 13880−13897

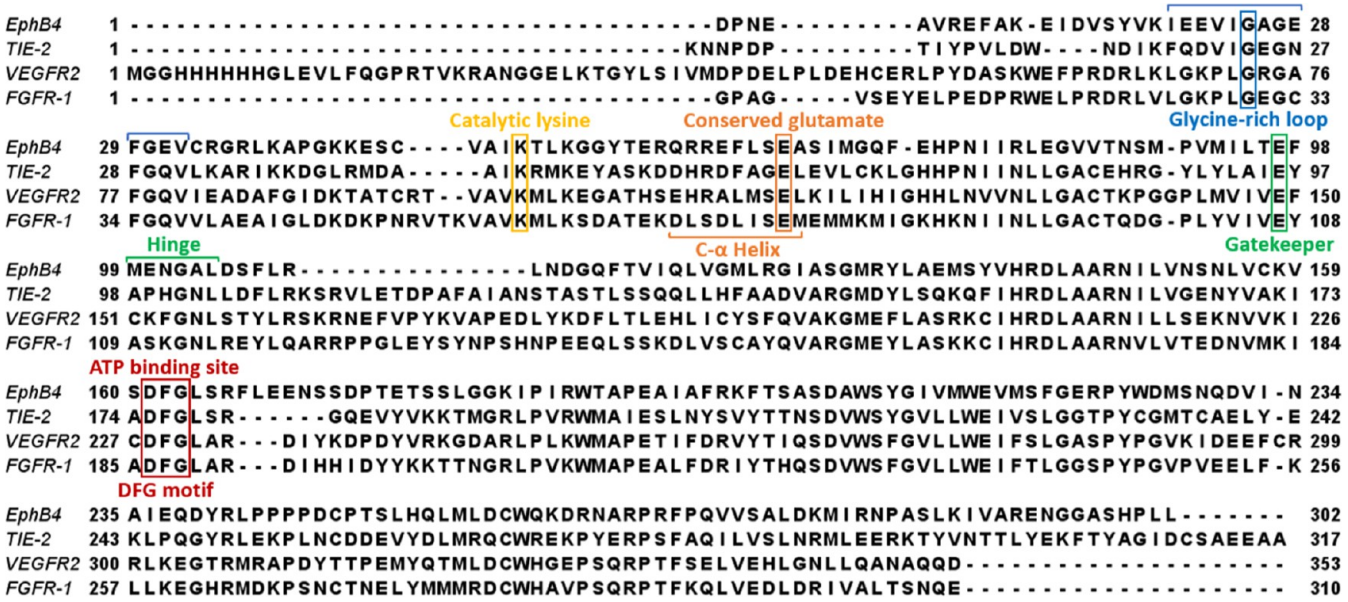

Figure 5. Multiple sequence alignment of four receptor tyrosine kinases representing the glycine-rich loop, hinge region, catalytic lysine, conserved glutamate, gatekeeper, and DFG motif.

3. RESULTS AND DISCUSSION

3.1. Protein Structural Alignment. To assess the rationale for finding potential multitargeted inhibitors, the structural similarities of VEGFR2, EphB4, FGFR-1, and TIE-2 domains in the protein sequence and structure were initially investigated. The multiple protein sequence similarities of VEGFR2, EphB4, FGFR-1, and TIE-2 have higher similar identities in all motifs and domains (Figure 4). The sequence alignment between VEGFR2 and EphB4, FGFR-1, and TIE-2 showed similarities of 34.88, 37.38, and 32.28%, respectively. The various domains such as the glycine-rich loop, conserved glutamate, gatekeeper domain, hinge region, and DFG motif are globally conserved and have high topological alignment patterns at different residual positions.

Based on the protein sequence residue positions (Figure 5), glycine-rich loop residues are positioned as follows: VEGFR2 at position 73, EphB4 at position 25, FGFR-1 at position 30, and TIE-2 at position 24. The catalytic lysine residues are located at position 102 in VEGFR2, position 54 in EphB4, position 59 in FGFR-1, and position 54 in TIE-2. The conserved glutamate residues at the C-α helix are positioned at 119 in VEGFR2, 71 in EphB4, 76 in FGFR-1, and 71 in TIE-2. The gatekeeper residues are found at position 149 in VEGFR2, position 97 in EphB4, position 107 in FGFR-1, and position 96 in TIE-2. Lastly, the DFG motifs are located between residue positions 228 and 230 in VEGFR2, 161 and 163 in EphB4, 186 and 188 in FGFR-1, and 175 and 177 in TIE-2.

The crystallographic structural alignment of these proteins also shows the lowest RMSD (Figure 6). The RMSD of protein structural alignment between VEGFR2 and FGFR-1 is 1.762 Å (Figure 7A), between VEGFR2 and TIE-2 is 1.543 Å (Figure 7B), between VEGFR2 and EphB4 is 1.914 Å (Figure 7C), between EphB4 and FGFR-1 is 1.965 Å (Figure 7D), between FGFR-1 and TIE-2 is 1.914 Å (Figure 7E), and between EphB4 and TIE-2 is 1.555 Å (Figure 7F).

The cocrystals of these crystallographic structures were inspected, and it was confirmed that they possess all interactions with the key residues of the DFG motif, C-α helix, gatekeeper, and hinge region (Figure 3). The active site of tyrosine protein kinases is divided into multiple subregions: the hinge region (front pocket), the gatekeeper area, the hinge region, conserved glutamate, and the hydrophobic allosteric back pocket. Here, we represented these critical residues surrounding the type-II cocrystallized ligands and their interaction plots (Figure S1), which are responsible for the angiogenesis catalytic activity. Based on the structural crystallographic residue positions, the hinge loop region is present in Cys919, Met696, Ala564, and Ala905 of VEGFR2, EphB4, FGFR-1, and TIE-2 proteins, respectively. The DFG-out motif is present in (Asp1046-Phe1047-Gly1048), (Asp768-Phe759-Gly760), (Asp641-Phe642-Gly643), and (Asp982-Phe983-Gly984) of VEGFR2, EphB4, FGFR-1, and TIE-2 proteins, respectively. The conserved glutamate is present in the C-α helix-bearing residues Glu885, Glue664, Glu531, and Glu872 of VEGFR2, EphB4, FGFR-1, and TIE-2 proteins, respectively. The gatekeeper conserved glutamate residue is adjacent to the hinge loop residue of Glu917, Glu562, Glu694, and Glu903 of VEGFR2, EphB4, FGFR-1, and TIE-2 proteins, respectively. To develop promising type-II antiangiogenesis, ideally, inhibitors should form polar hydrogen-bonding interactions with the hinge region residue and gatekeeper area residue and hydrophobic interactions with the hydrophobic back pocket projecting toward DFG-out conformations in all tyrosine kinase domains.

3.2. Pharmacophore Hypothesis Development and Validation. The e-pharmacophore hypothesis has been developed using the receptor−ligand complex of all proteins composed of up to seven pharmacophoric features (Figure 8). Among these seven features, we considered features that interact with the hinge C-α, DFG motif, and gatekeeper residues (Figure 9). The hypothesis is drawn from the binding interaction pattern of cocrystal type-II inhibitors with these residues. The developed pharmacophore hypothesis of the VEGFR2 e-pharmacophore complex has two HBA and two HBD features. The e-pharmacophore features of the EphB4 and FGFR-1 complexes have two HBA and one HBD features. The e-pharmacophore features of the TIE-2 complex have two HBA and two HBD features. Targeting these residues can

https://doi.org/10.1021/acsomega.4c08366
ACS Omega 2025, 10, 13880−13897

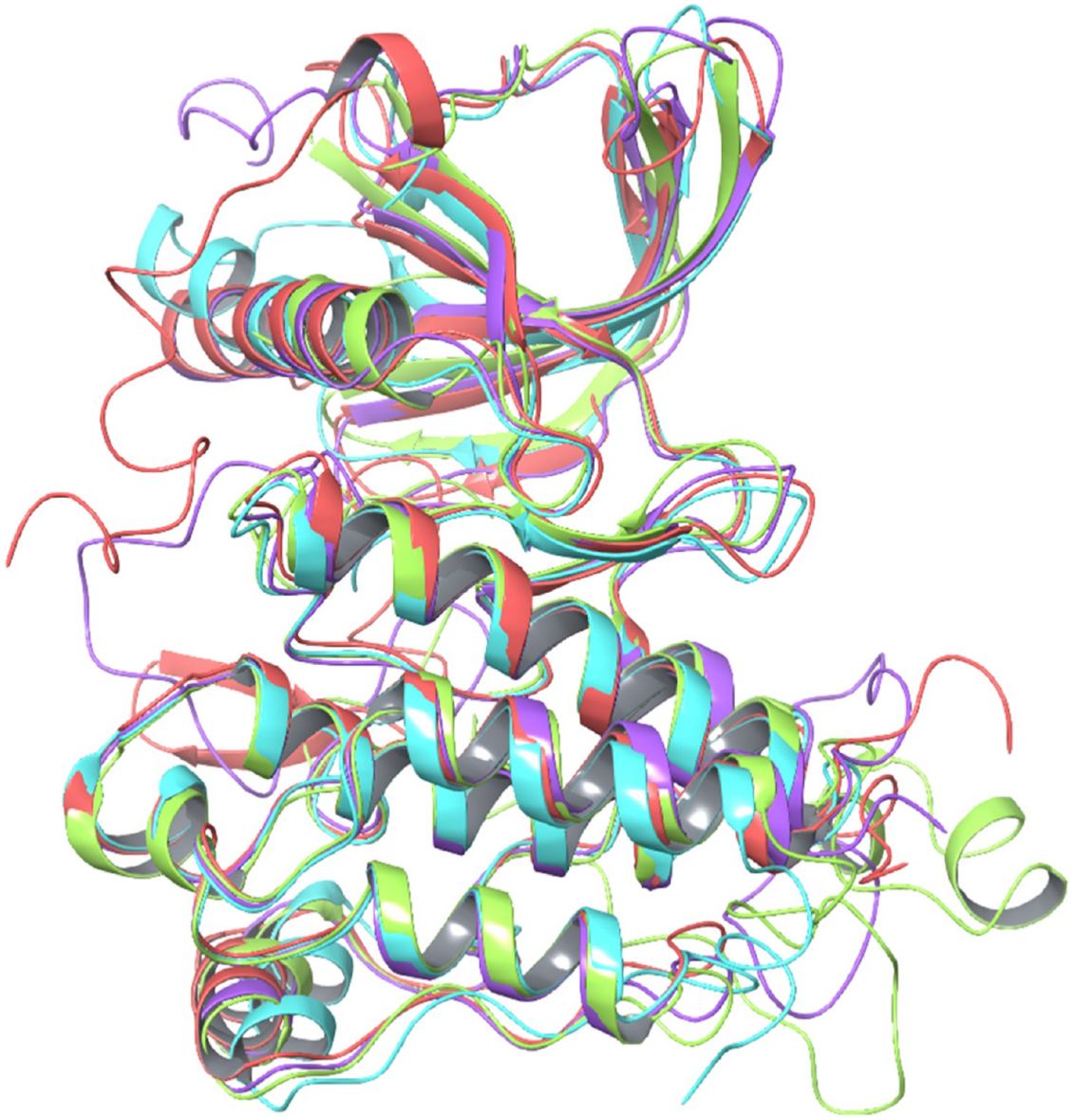

Figure 6. Superposition of the protein backbone VEGFR2, EphB4, FGFR-1, EphB4, and TIE-2, which are represented in salmon red, cyan, violet, and lime green colors, respectively.

result in exploring natural compound databases having identical binding patterns as those of cocrystals.

The test set of active inhibitors and decoys was constructed from the DUD-E and DEKOIS databases and was considered to validate the performance of the developed pharmacophoric models. The test sets were constructed at about 30:1 to mimic the natural chemical space ratio between active and inactive compounds. The test set of VEGFR2 contains 1240 compounds, of which 39 are active and 1201 are decoys. The test set of EphB4 contains 1240 compounds, including 40 active decoys and 1200 decoys. The test set of FGFR-1 contains 8846 compounds, including 146 active and 8700 decoys. The test set of TIE-2 contains 1240 compounds, including 40 active and 1200 decoys. The hypothesis validation function of the phase module and the active and decoy sets were imported for the partial matches of generated pharmacophoric features of all e-pharmacophore complexes. The statistical parameters such as EF, RIE, BEDROC, AUAC, and ROC were estimated based on the respective active and decoy data sets. Based on these parameters, we can recognize active sets in early recognition and discourage random selection. The enrichment analysis of these statistical parameters showed confidence in validated hypothesis models (Table 1).

3.3. Receptor-Based Guided Pharmacophoric Screening. To explore the curated databases and find accurate natural compounds that can bind with the essential residues, validated pharmacophore hypothesis models were aligned to interact with maximum common pharmacophoric features (Figure 10). These commonly aligned features were projected toward the DFG-out, hinge, and gatekeeper residues intended for this study. The screened natural compounds against VEGFR2, EphB4, FGFR-1, and TIE-2 hypothesis models gave 2846, 887, 432, and 349 compounds, respectively. The final survived hits from all targets were compared against each other to search for common natural compounds, which resulted in 217 compounds. These compounds had random alignment and fitness scores. To confirm the validated virtual screening, these

https://doi.org/10.1021/acsomega.4c08366
ACS Omega 2025, 10, 13880−13897

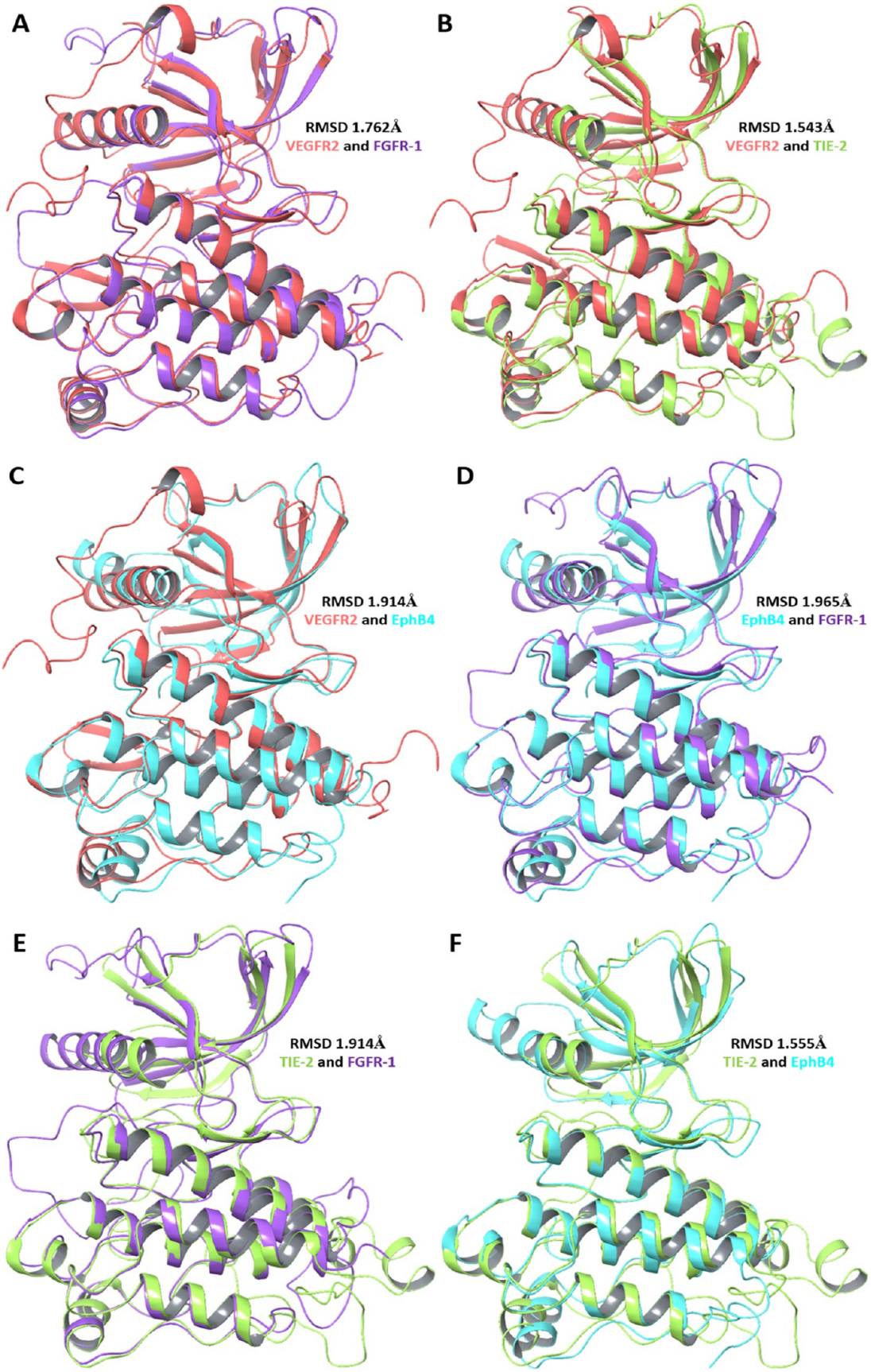

Figure 7. Pairwise structural alignment of VEGFR2, FGFR-1, EphB4, and TIE-2. The protein structural alignments between (A) VEGFR2 and FGFR-1, (B) VEGFR2 and TIE-2, (C) VEGFR2 and EphB4, (D) EphB4 and FGFR-1, (E) FGFR-1 and TIE-2, and (F) EphB4 and TIE-2 are represented based on their RMSD.

https://doi.org/10.1021/acsomega.4c08366
ACS Omega 2025, 10, 13880−13897

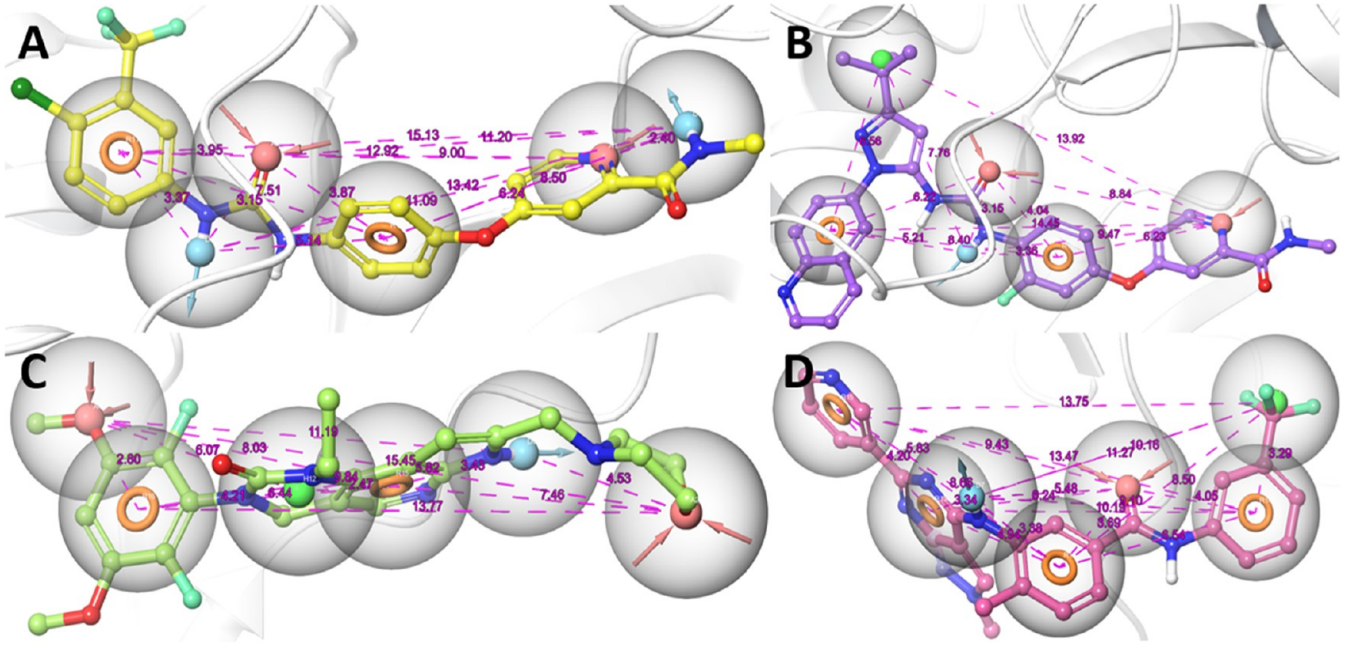

Figure 8. Receptor-based pharmacophore hypothesis showing the features of (A) VEGFR2, (B) EphB4, (C) FGFR-1, and (D) TIE-2 complexes.

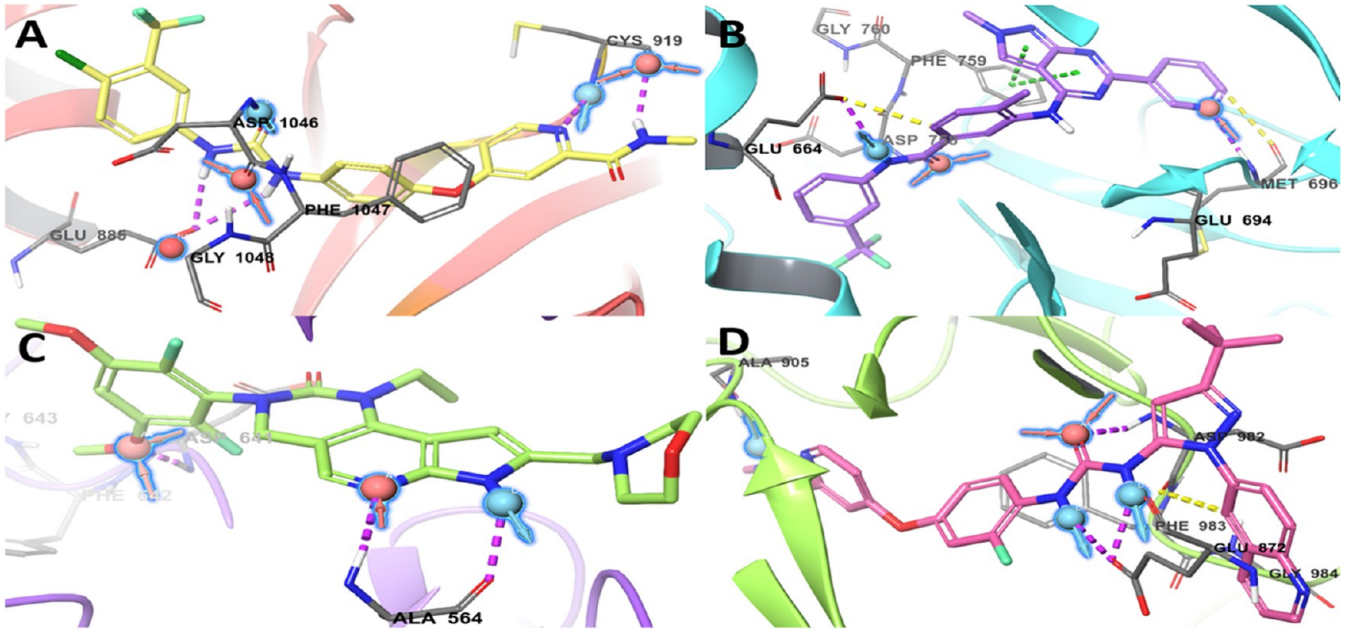

Figure 9. Developed residue-based pharmacophore (receptor−ligand cavity) hypothesis models of (A) VEGFR2, (B) EphB4, (C) FGFR-1, and (D) TIE-2 complexes.

Table 1. Enrichment Analysis of Validated E-Pharmacophore Hypothesis Models

sr. no.	hypothesis	EF%	BEDROC	ROC	AUAC
1	VEGFR2	18.98	0.88	0.95	0.94
2	EphB4	22.43	0.91	0.96	0.98
3	FGFR-1	15.18	0.95	0.93	0.89
4	TIE-2	8.63	0.88	0.90	0.82

compounds were further trimmed based on their fitness score, achieving a score of more than 1.0. The resulting 17 compounds might have potential multiangiogenic inhibition (Table 2), which were assessed for molecular interactions and binding affinity studies.

3.4. Molecular Docking. To mimic the accurate poses of the cocrystallized ligands and their molecular interactions at the active binding pocket, the validation of cocrystals is the foremost step before carrying out the intended molecular docking studies to estimate their RMSD and binding affinities. In addition to the binding affinities, we also considered the nonbonded energy (NBE) parameter to assess the suitable druglike candidate. The NBE estimates the flexibility restrictions of the ligand to fit accurately inside the active binding site conferred due to either the electrostatic or van der Waals interactions.[65−67] The hydrogen bonding (ΔG_{Hbond}) is

https://doi.org/10.1021/acsomega.4c08366
ACS Omega 2025, 10, 13880−13897

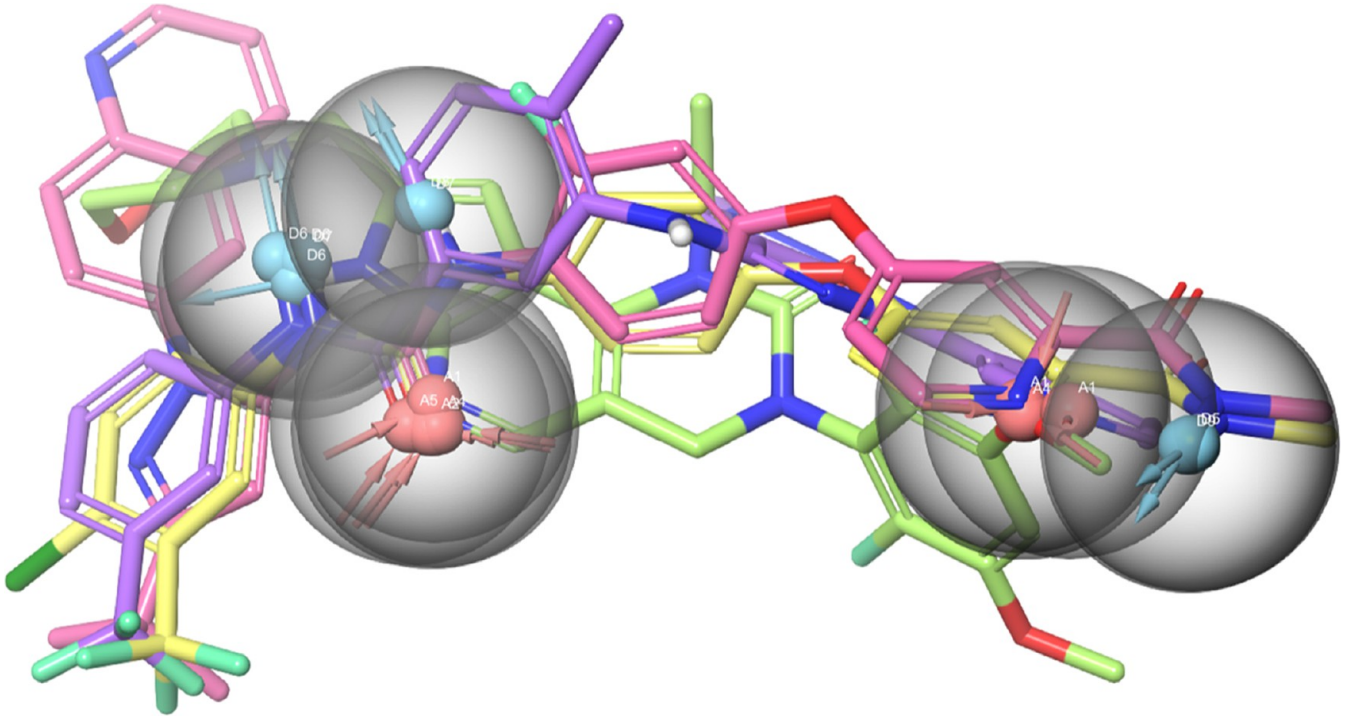

Figure 10. Developed e-pharmacophore hypothesis alignment between all.

Table 2. Best Common Hits Screened Out from the Aligned E-Pharmacophores

	align score				fitness score			
cmpd.	VEGFR2	EphB4	FGFR-1	TIE-2	VEGFR2	EphB4	FGFR-1	TIE-2
CNP0380350	0.109	0.317	0.183	0.063	2.552	2.101	1.634	2.590
CNP0415325	0.963	0.922	0.504	0.925	1.782	1.230	1.897	1.070
CNP0123154	1.031	0.118	0.224	0.780	0.636	1.958	1.476	1.217
CNP0003920	0.180	0.104	0.361	0.788	1.633	1.941	1.689	1.198
CNP0124351	0.972	0.334	0.408	0.836	1.834	1.440	1.911	1.176
CNP0258516	1.434	0.906	0.171	0.889	1.372	1.398	2.010	1.205
CNP0231313	0.880	0.112	0.779	0.577	1.959	2.080	1.625	1.346
CNP0303006	0.751	0.322	0.266	0.769	1.374	1.920	1.636	1.252
CNP0243075	0.821	0.237	0.246	0.771	1.909	1.734	1.592	1.381
CNP0227869	0.681	0.306	0.128	0.534	1.406	2.002	2.140	1.366
CNP0267500	0.532	0.298	0.388	0.391	1.445	1.825	1.854	1.405
CNP0392796	0.972	0.529	0.171	0.378	1.054	1.098	1.777	1.409
CNP0408548	0.665	0.366	0.560	0.879	1.131	1.516	1.756	1.460
CNP0286431	0.553	0.513	0.441	0.274	1.669	1.847	1.859	1.492
CNP0345218	1.266	0.183	0.469	0.457	1.472	1.989	1.769	1.528
CNP0344203	0.433	0.831	0.733	0.412	1.497	1.329	0.870	1.775
CNP0211397	0.431	0.350	0.756	0.410	1.611	1.942	1.310	1.913

essential due to the formation of polar contacts with the DFG-out motif and the gatekeeper glutamate residue. The lipophilic (ΔG_{lipo}) contacts are essential for interactions with the conserved lysine and C-α helix hinge loop residues. Hence, the binding affinity components of these parameters are also considered in this present study. The cocrystallized ligands were redocked with their respective tyrosine kinase proteins and their binding affinities were computed for comparison with the database used in this study. The redocked cocrystallized ligands successfully reproduced the identical binding pattern and achieved accurate poses (Figure 11) with the lowest RMSD, hence confirming the validation (Table 3). Moreover, the docked poses reproduced all of the essential interactions within active binding hotspots achieved by the cocrystallized ligands (Figure S1).

Molecular docking simulations were carried out for the 17 common compounds to evaluate their molecular binding patterns and interactions against all four drug targets to validate their proposed quartet inhibitory activity. All 17 compounds achieved accurate poses and the lowest RMSD within the binding cavity. Despite the compounds having aligned scores and good fitness scores, few compounds were able to show improved binding scores and affinities. The docking scores of 17 natural compounds were showing with a range of −6.494 to −12.540 kcal/mol, −5.572 to −13.683 kcal/mol, −3.026 to −10.495 kcal/mol, and −6.486 to −13.465 kcal/mol of VEGFR2, EphB4, FGFR-1, and TIE-2,

https://doi.org/10.1021/acsomega.4c08366
ACS Omega 2025, 10, 13880−13897

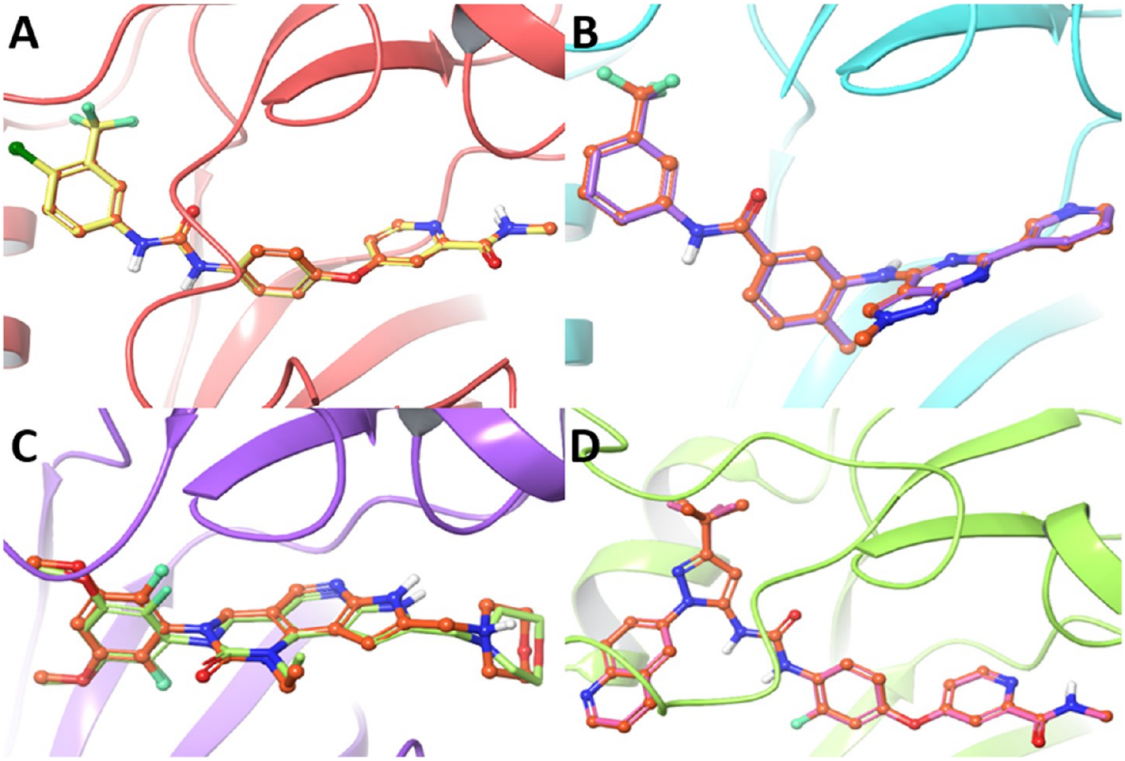

Figure 11. Redocked cocrystal conformers (in orange) superimposed on the cocrystallized ligands of (A) VEGFR2, (B) EphB4, (C) FGFR-1, and (D) TIE-2 PDB complexes.

Table 3. Redocked Score and Binding Affinities (kcal/mol) of Protein Complexes

proteins	cocrystal	GScore	MM-GBSA	NBE	ΔG_{Hbond}	ΔG_{lipo}	RMSD (Å)
VEGFR2	sorafenib	−12.286	−94.28	−71.92	−2.68	−15.85	0.145
EphB4	NVP-BHG712	−13.138	−106.75	−63.92	−2.78	−19.85	0.105
FGFR-1	pemiganitib	−7.350	−92.34	−70.92	−3.87	−21.85	0.009
TIE-2	DP1919	−12.894	−102.10	−63.16	−1.64	−19.14	0.177

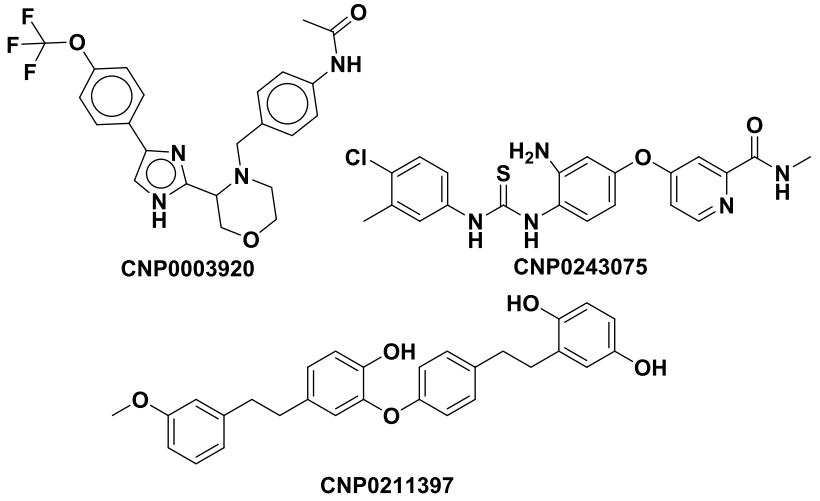

Figure 12. Best-selected compounds for molecular dynamics and ADMET assessment.

respectively. From the overall docking scores and binding affinity results, compounds CNP0003920, CNP0243075, and CNP0211397 (Figure 12) were found to have higher scores than the cocrystallized ligands (Table 4). These three compounds were estimated for the per-residue energy decomposition based on their hydrogen and hydrophobic interactions. The molecular binding interactions of natural compounds showed consistent residual interacting energies (Figures S2−S4). This is due to their accurate superimposition (Figures S5−S7), thus possessing higher energies over the cocrystallized ligands (Tables S1−S4).

https://doi.org/10.1021/acsomega.4c08366
ACS Omega 2025, 10, 13880−13897

Table 4. Docking Score and MM-GBSA of Hits from the Common Pharmacophores

	GScore (kcal/mol)				MM-GBSA (kcal/mol)			
cmpd.	VEGFR2	EphB4	FGFR-1	TIE-2	VEGFR2	EphB4	FGFR-1	TIE-2
CNP0380350	−12.214	−8.766	−4.107	12.504	−100.26	−82.54	−64.47	−86.30
CNP0415325	−8.800	−9.250	−10.205	−10.594	−69.39	−60.69	−79.68	60.48
CNP0123154	−8.480	−9.882	−6.534	−8.847	−52.97	−68.44	−86.16	−66.83
CNP0003920	−12.344	−13.035	−9.107	−12.545	−100.81	−106.02	−92.34	−112.10
CNP0124351	−7.676	−5.709	−7.078	−7.796	−50.92	−60.94	−69.90	−66.11
CNP0258516	−10.474	−6.555	−4.352	−9.727	−63.51	−68.46	−67.64	−60.53
CNP0231313	−8.484	−7.466	−7.730	−8.906	−62.87	−71.65	−67.85	−77.44
CNP0303006	−8.723	−10.262	−5.948	−9.757	−51.50	−74.34	−112.53	−70.16
CNP0243075	−12.358	−13.617	−8.626	−12.137	−104.28	−107.85	−94.82	−116.44
CNP0227869	−10.043	−7.538	−9.193	−10.084	−60.26	−69.99	−74.17	−70.66
CNP0267500	−10.497	−8.890	−3.026	−9.569	−67.60	−80.05	−70.82	−70.97
CNP0392796	−10.594	−5.572	−7.411	−12.083	−72.03	−73.35	−74.32	−77.02
CNP0408548	−6.494	−7.329	−7.675	−6.486	−59.85	−61.99	−74.36	−68.96
CNP0286431	−10.760	−9.782	−7.281	−11.283	−71.31	−76.49	−78.03	−90.29
CNP0345218	−9.240	−8.069	−4.030	−9.539	−62.78	−65.93	−71.76	−73.21
CNP0344203	−10.086	−8.963	−5.868	−8.387	−69.76	−85.54	−87.53	−69.42
CNP0211397	−12.540	−13.683	−10.495	−13.465	−103.83	−109.85	−92.94	−116.28

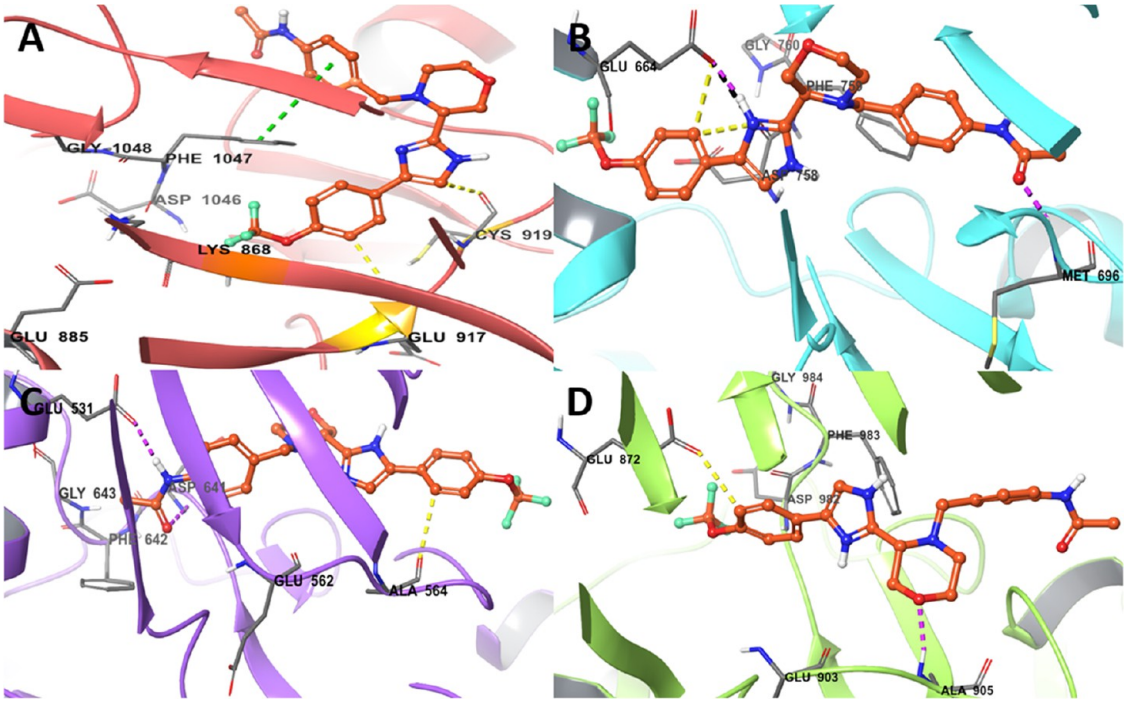

Figure 13. Molecular interactions between CNP0003920 (in orange) with (A) VEGFR2, (B) EphB4, (C) FGFR-1, and (D) TIE-2 proteins.

The morpholine and imidazole rings of CNP0003920 formed polar hydrogen bonds with the conserved glutamate gatekeeper residues Glu917 (−57.90 kcal/mol), Glu664 (−56.97 kcal/mol), Glu531 (−60.40 kcal/mol), and Glu872 (−50.98 kcal/mol), which are having higher than the cocrystal binding with Glu917 (−58.21 kcal/mol), Glu664 (−56.31 kcal/mol), Glu562 (−61.80 kcal/mol), and Glu903 (−59.26 kcal/mol) of VEGFR2, EphB4, FGFR-1, and TIE-2, respectively (Figure 13). The hinge region residue forming hydrogen bonds with Cys919 (−30.14 kcal/mol), Met696 (−36.97 kcal/mol), Ser565 (−28.81 kcal/mol), and Ala905 (−20.68 kcal/mol) has good binding energies as those of cocrystals Cys919 (−32.67 kcal/mol), Met696 (−37.91 kcal/mol), and Ala905 (−21.44 kcal/mol) of VEGFR2, EphB4, and TIE-2, respectively. Interestingly, no formation of polar contacts has been observed in the FGFR-1 complex with the hinged Ser565 residue. Similarly, the distal carboxamide moiety participates in aromatic hydrogen bonding and $\pi-\pi$ stacking with Phe1047 and Phe642 of the DFG motif in VEGFR2 and FGFR-1, respectively, in addition to Asp758 (−55.57 kcal/mol) and Asp641 (−61.90 kcal/mol) of EphB4, FGFR-1, and TIE-2 proteins, respectively.

The carboxamide group at the third position of the distal pyridine ring exhibited polar hydrogen contacts with the conserved glutamate gatekeeper residues Glu917 (−60.99 kcal/mol), Glu664 (−58.97 kcal/mol), and Glu872 (−56.66 kcal/mol), whereas the cocrystals binding with Glu917 (−60.99 kcal/mol), Glu664 (−58.97 kcal/mol), and Glu872

https://doi.org/10.1021/acsomega.4c08366
ACS Omega 2025, 10, 13880−13897

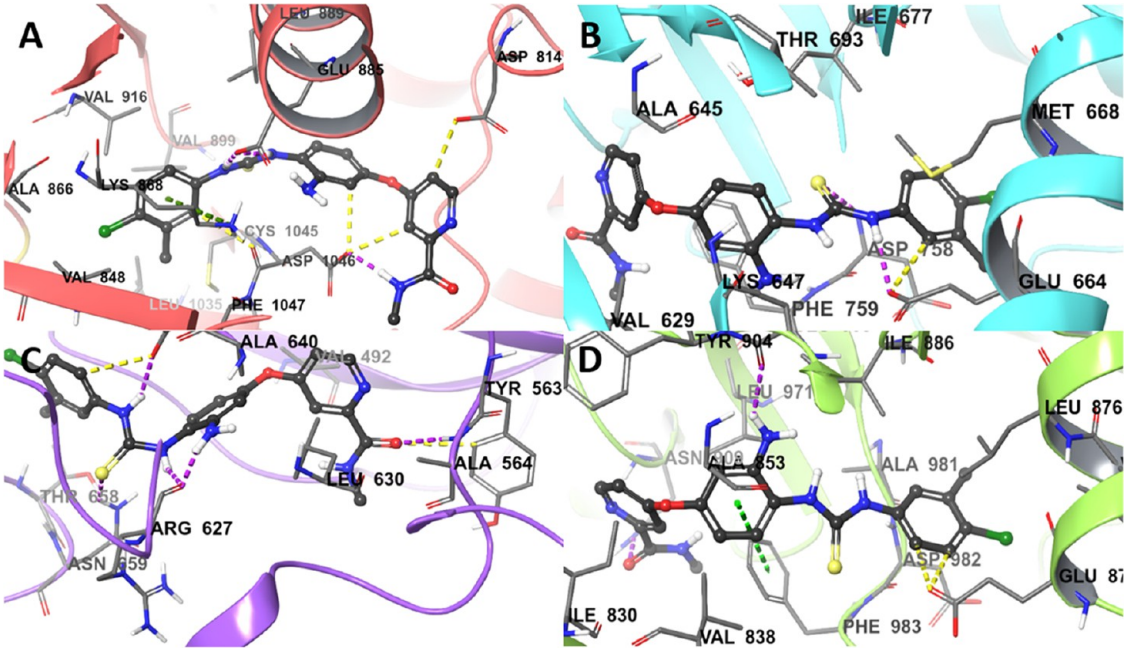

Figure 14. Molecular interactions between CNP0243075 (black) with (A) VEGFR2, (B) EphB4, (C) FGFR-1, and (D) TIE-2 proteins.

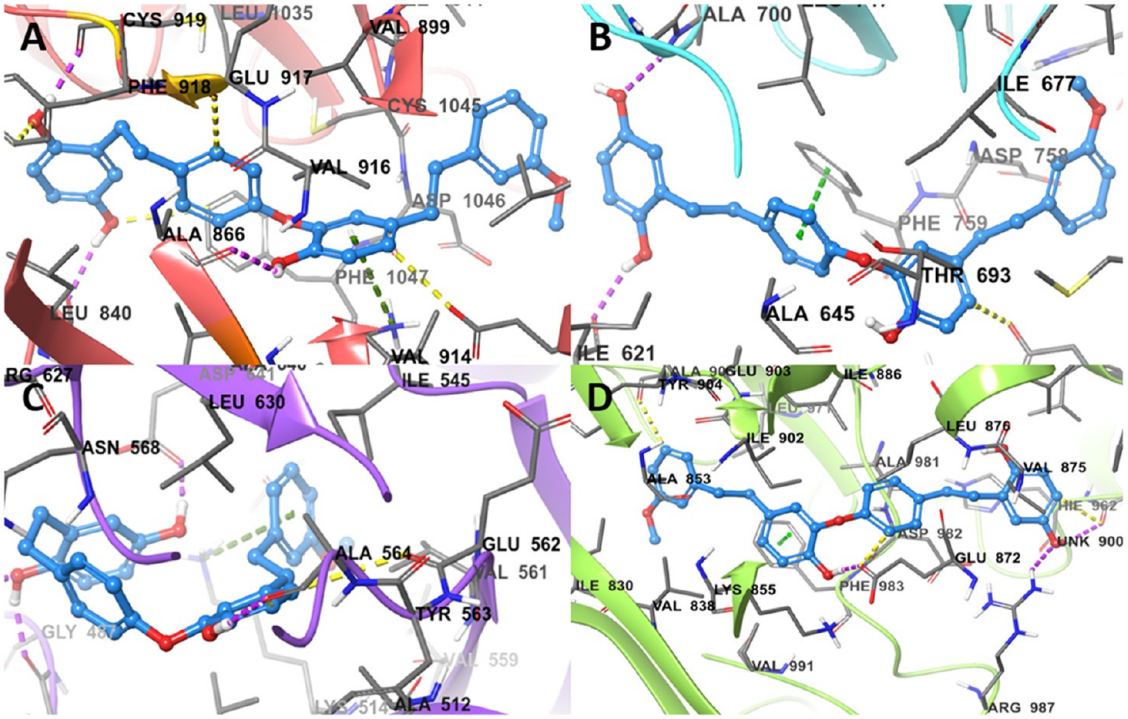

Figure 15. Molecular interactions between CNP0211397 (in blue) and (A) VEGFR2, (B) EphB4, (C) FGFR-1, and (D) TIE-2 proteins.

(−54.29 kcal/mol) of VEGFR2, EphB4, and TIE-2, respectively (Figure 14). The hinge region residue forms hydrogen bonds with Cys919 (−28.71 kcal/mol), Met696 (−37.28 kcal/mol), Ser565 (−29.10 kcal/mol), and Ala905 (−18.78 kcal/mol), having good binding energies as those of cocrystals Cys919 (−32.67 kcal/mol), Met696 (−37.91 kcal/mol), and Ala905 (−21.44 kcal/mol) of VEGFR2, EphB4, and TIE-2, respectively. Interestingly, additional formation of polar contacts has been observed in the FGFR-1 complex with the hinge Ser565 residue. Similarly, the chloro-substituted phenyl ring occluded toward the outside, forming hydrophobic interactions with Asp1046 (−58.62 kcal/mol), Asp641 (−60.94 kcal/mol), and Asp982 (−60.67 kcal/mol) of VEGFR2, FGFR-1, and TIE-2, respectively. Besides the DFG binding motif, additional $\pi-\pi$ stacking was observed with Phe1047 (−36.86 kcal/mol) and the π-cation with Arg987 (−59.90 kcal/mol).

The gatekeeper glutamate residue exhibiting hydrogen bonding with Glu918 (−58.03 kcal/mol), Glu664 (−55.42), and Glu872 (−54.54 kcal/mol) showed higher binding than Glu917 (−58.21 kcal/mol) and Glu903 (−59.26 kcal/mol) of VEGFR2 and TIE-2, respectively (Figure 15). The hinge

https://doi.org/10.1021/acsomega.4c08366
ACS Omega 2025, 10, 13880−13897

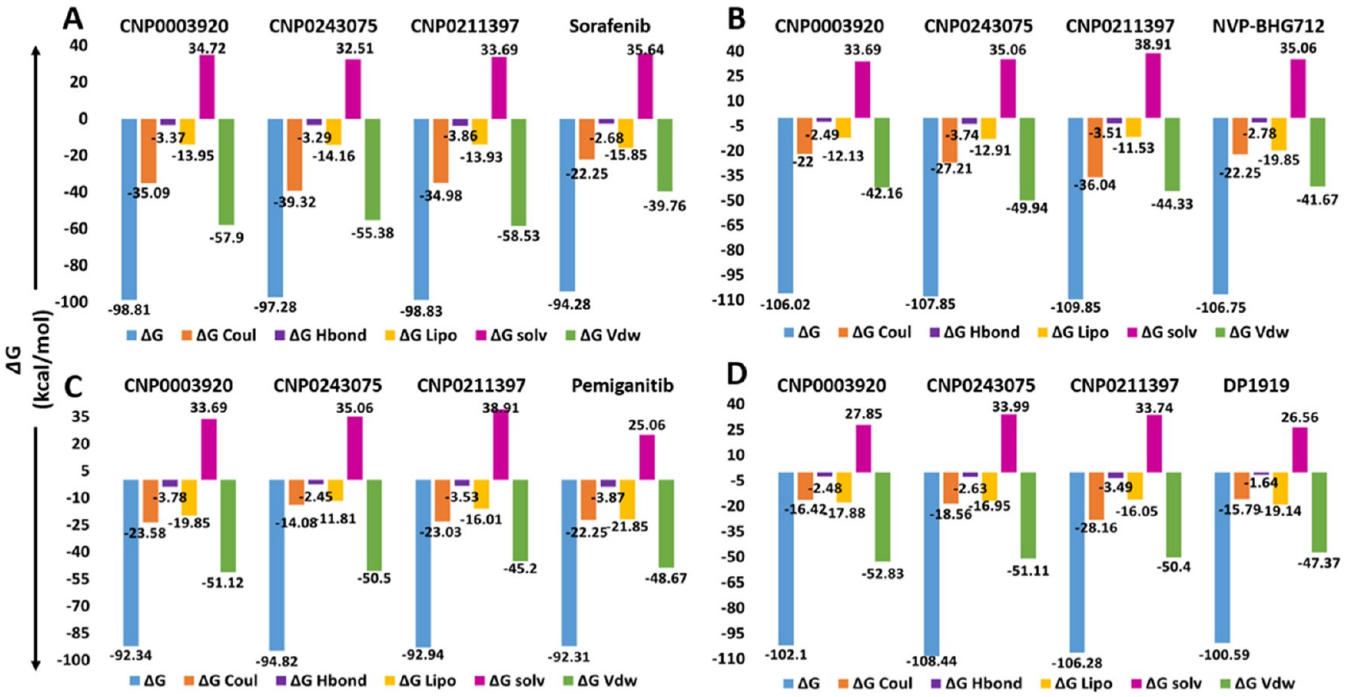

Figure 16. Binding affinities of best-selected natural compounds and the standard control against (A) VEGFR2, (B) EphB4, (C) FGFR-1, and (D) TIE-2 proteins.

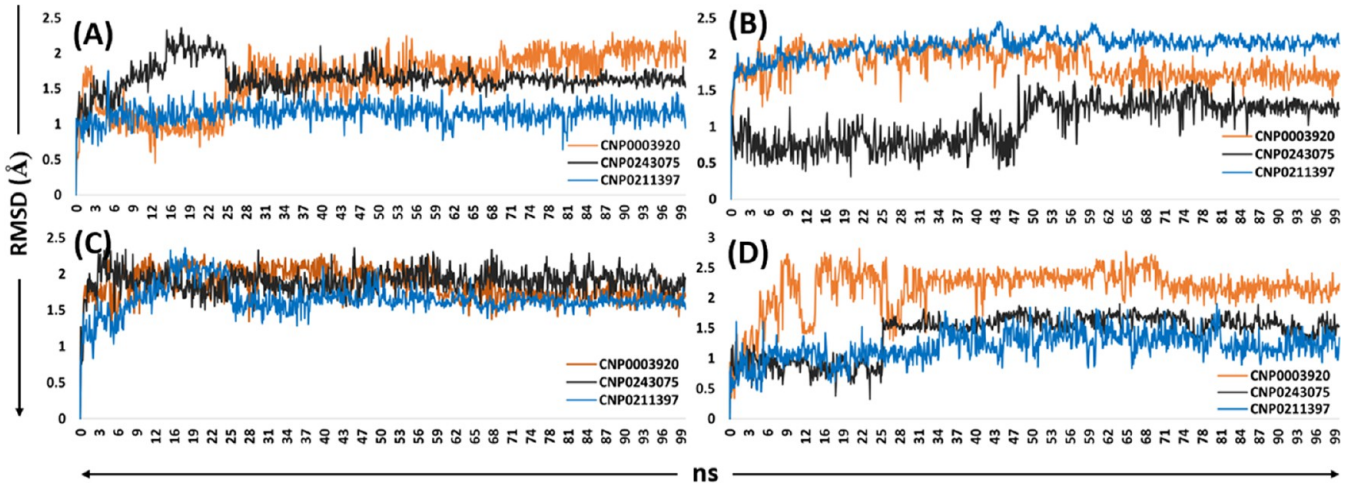

Figure 17. RMSD trajectories of CNP0003920, CNP0243075, and CNP0211397 complexed with (A) VEGFR2, (B) EphB4, (C) FGFR-1, and (D) TIE-2 proteins.

region residue forming hydrogen bonds with Met696 (−38.90 kcal/mol), Ser565 (−28.34 kcal/mol), and Ala905 (−21.56 kcal/mol) showed similar binding patterns as those of cocrystals Met696 (−37.91 kcal/mol) and Ala905 (−21.44 kcal/mol) of EphB4, FGFR-1, and TIE-2, respectively. The central phenyl moiety of CNP0211397 has been crucial for forming interactions with the DFG-out binding motif. Specifically, the DFG-out residues Asp1046 of VEGFR2 (−58.69 kcal/mol), Asp758 of EphB4 (−53.90 kcal/mol), and Asp982 of TIE-2 (−60.55 kcal/mol) contribute significantly to these interactions.

From the binding interaction analysis, the phenyl carboxamide ring fits in the gatekeeper area stabilized via hydrogen-bonding interactions. The imidazole ring actively interacts with side-chain carboxylate of glutamate residues of the αC helix and aspartate residues of the conserved DFG motif. The substituted aryl moieties are accommodated and projected toward the hinge region interacting with most of the target compounds through hydrogen bonding. A few key hydrophobic interactions, such as Val848, Ala866, Val916, and Leu1035 of VEGFR2; Ala645, Phe671, Ile677, Val629, Met668, and Thr693 of EphB4; Val492, Ile545, Leu630, Ala640, Ala512, and Val561 of FGFR-1; and Leu971, Ala981, Leu876, Ile830, and Ala853 of TIE-2, were involved with the side chains in the hinge region and toward the allosteric back pocket. Many reports corroborate our docking simulation findings that the presence of aryl groups such as morpholine,[68,69] pyridine,[70,71] fluorophenyl,[72,73] carboxamide-based scaffolds,[74] and urea[68,75−77] has a great potential for the development of antiangiogenic inhibitors. Hence, the selected natural compounds from the developed and validated pharmacophore hypothesis models confirm the potential role

https://doi.org/10.1021/acsomega.4c08366
ACS Omega 2025, 10, 13880−13897

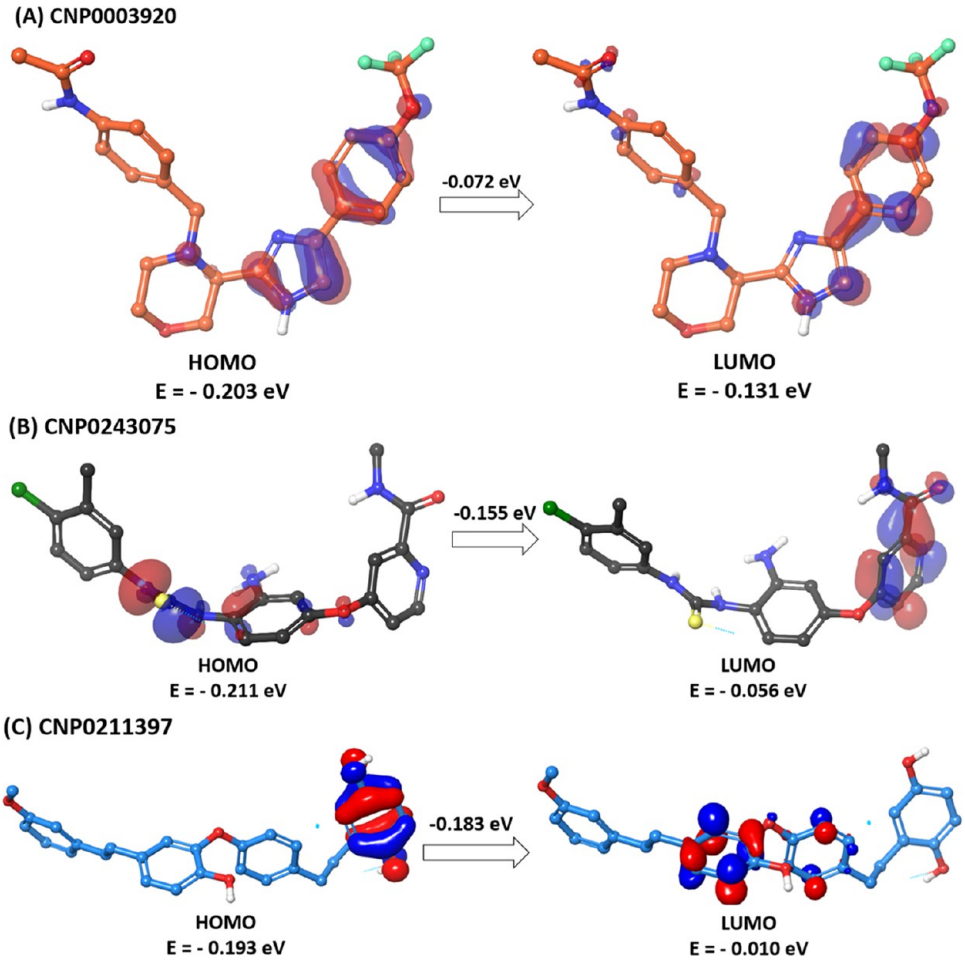

Figure 18. Frontier molecular orbitals of potent hits representing the electronic energies of the HOMO and LUMO. The energy gaps between the HOMO and the LUMO are represented on the arrow.

of angiogenesis inhibitors. Further, a comparative binding affinity assessment was made for these compounds with the cocrystallized ligands (Figure 16). The binding components such as ΔG_{Hbond}, ΔG_{lipo}, ΔG_{Solv} (solvation energy), and nonbonded energies (ΔG_{coul} and ΔG_{vdW}) were showing higher binding affinities than the cocrystals.

3.5. Molecular Dynamics Simulations. The molecular dynamics simulations were performed in triplicate for up to 100 ns and their deviations were small and nonsignificant. All of the complexed ligands showed a consistent RMSD throughout the simulation course (Figure 17). Initially, a few distortions were observed for up to 30 ns, especially with the CNP0003920 and CNP0243075 ligands. This could be due to the proper adjustment of compactness for stabilization inside the binding pocket. The RMSD of complexes with the CNP0003920 ligand plateaued until equilibration was achieved within the first 30 ns, and they ceased undergoing significant conformational changes. The average RMSDs achieved were 1.86 ± 0.21 Å, 1.89 ± 0.17 Å, 1.65 ± 0.20 Å, and 2.16 ± 0.37 Å with VEGFR2, EphB4, FGFR-1, and TIE-2, respectively. Similarly, CNP0243075 also exhibited a few distortions, indicating that the ligand attempts to maintain its accurate pose stability inside the pocket. The CNP0003920 ligand bound with proteins achieved average RMSDs of 2.13 ± 0.18 Å, 1.50 ± 0.33 Å, 2.02 ± 0.37 Å, and 1.46 ± 0.20 Å with VEGFR2, EphB4, FGFR-1, and TIE-2, respectively. In contrast to these two ligands, CNP0211397 showed a better RMSD and pose stability that maintained average RMSDs of 1.21 ± 0.14 Å, 2.20 ± 0.13 Å, 1.89 ± 0.17 Å, and 1.14 ± 0.13 Å with VEGFR2, EphB4, FGFR-1, and TIE-2, respectively.

3.6. Density Functional Theory. The frontier molecular spin orbitals HOMO and LUMO of chemical species are essential for the reactivity and stability of the protein−ligand interaction. The HOMO energy represents the inhibitors that can donate electrons during the protein complex formation, while the LUMO energy manifests the inhibitors to accept the electrons from the enzymes. The orbital energy of stable hit molecules is computed using DFT. The frontier between HOMO and LUMO energy orbitals enumerated the excitation energy of the electrons. The correlation of higher binding affinities concerning the electronic energies suggests that the HOMO electrons transfer to the lower LUMO in the active site of proteins. The HOMO−LUMO energy gap of all hits was very less significant between −0.072 and −0.182 eV (Figure 18). The electronic densities around the nuclei surface are expressed by the MESP. The negative surface (red) signifies the electron-rich regions, and the positive surface (blue) signifies the electron-deficient regions. The MESP exhibited low and high electron densities, which can correspond with the molecular interactions, which can be corroborated with our research findings. At the active binding site, these densities fall at the accurate region of the compound, which formed interactions with the catalytic ATP binding site (DFG motif), c-α residues at the hinge region, and conserved

https://doi.org/10.1021/acsomega.4c08366
ACS Omega 2025, 10, 13880−13897

glutamate residue. The MESP of compounds CNP0003920, CNP0243075, and CNP0211397 were −41.20, −36.78, and −43.38 kcal/mol, respectively.

3.7. Physicochemical and ADMET Assessment. The best-selected compounds CNP0003920, CNP0243075, and CNP0211397 were assessed for physicochemical and pharmacokinetic profiling (Table 5). All three compounds exhibited

Table 5. Physicochemical Properties and ADMET Assessment of CNP0003920, CNP0243075, and CNP0211397[a]

sr. no.	parameters	CNP0003920	CNP0243075	CNP0211397
1	molecular weight (g/mol)	460.17	441.94	482.08
2	hydrogen bond donor	2	3	3
3	hydrogen bond acceptor	7	7	7
4	no. of rotatable bonds	8	7	9
5	total polar surface area (Å)	79.48	135.46	92.35
6	solubility (mol/L)	−4.029	−3.015	−3.463
7	partition coefficient ($\log P_{o/w}$)	3.48	1.526	4.685
8	distribution coefficient ($\log D$)	3.107	1.961	3.81
9	Caco-2 permeability (cm/s)	−4.734	−5.113	−5.265
10	p-gp substrate	0.140	0.281	0.005
11	p-gp-inhibitor	0.031	0.003	0.971
12	human intestinal absorption	0.0	0.001	0.0
13	plasma protein binding (%)	95.106	57.867	89.237
14	volume of distribution (L/kg)	0.538	0.06	0.197
16	clearance (mL/min/kg)	4.981	4.528	2.549
17	half-life ($t_{1/2}$)	0.601	0.991	1.513
18	rat oral acute toxicity	0.277	0.743	0.357
19	cardiotoxicity	0.697	0.619	0.562
20	drug-induced liver injury	0.994	0.998	0.999
21	skin sensitization	0.004	0.177	0.133
22	carcinogenicity	0.409	0.862	0.065
23	eye irritation/corrosion	0.037	0.033	0.0
24	respiratory toxicity	0.621	0.515	0.502
25	AMES mutagenicity	0.265	0.853	0.398
26	hepatotoxicity	0.943	0.916	0.896
27	nephrotoxicity	0.998	0.924	0.991
28	hematotoxicity	0.4	0.742	0.766
29	genotoxicity	1.0	1.0	1.0
30	neurotoxicity	0.947	0.991	0.844

[a]Here, P-gp inhibitors/substrates, human intestinal absorption (HIA), metabolism, half-life, and toxicity are predicted in probability values scaled between 0 (poor) and 1 (excellent).

predicted solubility within the acceptable limits (0.5 to −4 log mol/L). The partition coefficient shows higher lipophilicity, exceeding the optimal range of 0−3 for the selected molecules. All compounds demonstrated favorable Caco-2 permeability. The predicted probability of being a P-gp substrate and an inhibitor is within optimum limits. The therapeutic window absorption (human intestinal absorption) is acceptable within the limits. This correlation can be attributed to the plasma protein binding (PPB) and blood plasma fractions, directly influencing human intestinal absorption. A higher PPB (>90%) results in a lower volume of drug distribution in blood plasma leading to a lower absorption rate. Compound CNP0003920 showed higher PPB compared to other selected compounds, which led to a lower drug distribution (0.538) and a higher clearance time (4.981). The half-life of the CNP0211397 compound was reasonably higher than others. In terms of toxicity parameters, based on the probability of all parameters, the selected compounds showed very low probability values and had lower adverse risks.

4. CONCLUSIONS

In the present study, we unveiled the simultaneous angiogenic inhibition profile using the NP-likeness database against multimodal VEGFR2, EphB4, FGFR-1, and TIE-2 inhibition using receptor-based pharmacophore modeling. The results showed that 17 common compounds mapped well onto the features of our designed pharmacophore models that could bind effectively with the gatekeeper, hinge, ATP-catalytic, and DFG motif residues. After thorough screening, three compounds CNP0003920, CNP0243075, and CNP0211397 were demonstrated to have better docking scores, binding modes, and favorable physiochemical and ADMET properties. These three compounds were then subjected to 100 ns long MD simulations to assess their molecular stability and binding energy using the MM-GBSA end-point method. However, after careful analysis of their stability inside the active binding pocket during molecular dynamics simulations, it was found that all compounds retained similar forms of stable interactions. In comparison with the reference clinical candidates sorafenib, NVP-BHG712, pemiganitib, and DP1919, the screened derived natural compounds can effectively target VEGFR2/EphB4/FGFR-1/TIE-2 proteins. These compounds are assumed to effectively block the angiogenesis pathway and reduce the angiogenesis process. The three derived NP-like candidates can be considered potential candidates for further exploration in designing novel quartet-kinase inhibitors. The biological evaluations of these compounds are still underway and will be reported elsewhere. Our results may contribute as a novel regimen to the discovery of novel antiangiogenesis chemotypes for the intervention of pathological angiogenesis-related diseases.

■ ASSOCIATED CONTENT

Supporting Information

The Supporting Information is available free of charge at https://pubs.acs.org/doi/10.1021/acsomega.4c08366.

Molecular interactions of VEGFR2, EphB4, FGFR-1, and TIE-2 PDB complexes (Figure S1); molecular interactions of CNP0003920 with VEGFR2, EphB4, FGFR-1, and TIE-2 proteins, respectively (Figure S2); molecular interactions of CNP0243075 with VEGFR2, EphB4, FGFR-1, and TIE-2 proteins, respectively (Figure S3); molecular interactions of CNP0211397 with VEGFR2, EphB4, FGFR-1, and TIE-2 proteins, respectively (Figure S4); molecular overlay between CNP0003920 and cocrystals of all proteins (Figure S5); molecular overlay between CNP0243075 and cocrystals of all proteins (Figure S6); molecular overlay between

https://doi.org/10.1021/acsomega.4c08366
ACS Omega 2025, 10, 13880−13897

CNP0211397 and cocrystals of all proteins (Figure S7); per-residue decomposition of selected natural compounds with VEGFR2 (Table S1); per-residue decomposition of selected natural compounds with EphB4 (Table S2); per-residue decomposition of selected natural compounds with FGFR-1 (Table S3); and per-residue decomposition of selected natural compounds with TIE-2 (Table S4) (PDF)

AUTHOR INFORMATION

Corresponding Authors

Amit K. Keshari − *Department of Pharmaceutical Chemistry, Amity Institute of Pharmacy, Amity University Uttar Pradesh, Lucknow Campus, Lucknow 226028 Uttar Pradesh, India;* orcid.org/0000-0002-9806-7427; Phone: +91-7054090169; Email: amitkeshari.pharma@gmail.com

Richie R. Bhandare − *Department of Pharmaceutical Sciences, College of Pharmacy and Health Sciences, Ajman University, Ajman 346, United Arab Emirates; Centre of Medical and Bio-allied Health Sciences Research, Ajman University, Ajman 346, United Arab Emirates*; Phone: +971-564873619; Email: r.bhandareh@ajman.ac.ae

Authors

Jeevan Patra − *Department of Pharmaceutical Chemistry, Amity Institute of Pharmacy, Amity University Uttar Pradesh, Lucknow Campus, Lucknow 226028 Uttar Pradesh, India*

Afzal B. Shaik − *Department of Pharmaceutical Sciences, School of Biotechnology and Pharmaceutical Sciences, Vignan's Foundation for Science, Technology & Research, Guntur 522213, India; Center for Global Health Research, Saveetha Medical College, Saveetha Institute of Medical and Technical Sciences, Chennai 600077, India;* orcid.org/0000-0002-9036-1963

Madison Parrot − *Division of Clinical Pharmacology, Department of Pediatrics, Spencer Fox Eccles School of Medicine and Department of Molecular Pharmaceutics, Utah Center for Nanomedicine, College of Pharmacy, University of Utah, Salt Lake City, Utah 84112, United States*

Shiru Lin − *Division of Chemistry and Biochemistry, Texas Woman's University, Denton, Texas 76204, United States;* orcid.org/0000-0002-0159-2269

Complete contact information is available at: https://pubs.acs.org/10.1021/acsomega.4c08366

Author Contributions

J.P.: conceptualization, investigation, computational studies, data analysis, and writing—original draft. A.K.K.: conceptualization, initiation, writing—original draft, review—manuscript, and project administration. R.R.B.: funding acquisition, review—manuscript, and data analysis. A.B.S.: data analysis and review—manuscript. M.P.: formal analysis and review—manuscript. S.L.: data analysis and review—manuscript. All authors are gratefully thankful to the potential reviewers for their constructive comments on the improvement of the overall manuscript.

Notes

The authors declare no competing financial interest.

ACKNOWLEDGMENTS

R.R.B. would like to thank the Deanship of Graduate Studies and Research at Ajman University for providing financial support for this manuscript.

REFERENCES

(1) Qin, S.; Li, A.; Yi, M.; Yu, S.; Zhang, M.; Wu, K. Recent advances on anti-angiogenesis receptor tyrosine kinase inhibitors in cancer therapy. *J. Hematol. Oncol.* **2019**, *12* (1), No. 27.

(2) Liu, Z.-L.; Chen, H.-H.; Zheng, L.-L.; Sun, L.-P.; Shi, L. Angiogenic signaling pathways and anti-angiogenic therapy for cancer. *Signal Transduction Targeted Ther.* **2023**, *8* (1), No. 198.

(3) Folkman, J.; Parris, E. E.; Folkman, J.; et al. Tumor angiogenesis: therapeutic implications. *N. Engl. J. Med.* **1971**, *285* (21), 1182−1186.

(4) Huang, L.; Huang, Z.; Bai, Z.; Xie, R.; Sun, L.; Lin, K. Development and strategies of VEGFR-2/KDR inhibitors. *Future Med. Chem.* **2012**, *4* (14), 1839−1852.

(5) Chioccioli, M.; Marsili, S.; Bonaccini, C.; Procacci, P.; Gratteri, P. Insights into the conformational switching mechanism of the human vascular endothelial growth factor receptor type 2 kinase domain. *J. Chem. Inf. Model.* **2012**, *52* (2), 483−491.

(6) Kappert, K.; Peters, K. G.; Böhmer, F. D.; Ostman, A. Tyrosine phosphatases in vessel wall signaling. *Cardiovasc. Res.* **2005**, *65* (3), 587−598.

(7) Modi, S. J.; Kulkarni, V. M. Vascular endothelial growth factor receptor (VEGFR-2)/KDR inhibitors: medicinal chemistry perspective. *Med. Drug Discovery* **2019**, *2*, No. 100009.

(8) Benjamin, L. E.; Keshet, E. Conditional switching of vascular endothelial growth factor (VEGF) expression in tumors: induction of endothelial cell shedding and regression of hemangioblastoma-like vessels by VEGF withdrawal. *Proc. Natl. Acad. Sci. U.S.A.* **1997**, *94* (16), 8761−8766.

(9) Shanchun, G.; Laronna, S. C.; Tanisha, Z. M.; Ruben, R. G.-P. Regulation of Angiogenesis in Human Cancer via Vascular Endothelial Growth Factor Receptor-2 (VEGFR-2). In *Tumor Angiogenesis*; Sophia, R., Ed.; IntechOpen: Rijeka, 2012.

(10) Hicklin, D. J.; Ellis, L. M. Role of the vascular endothelial growth factor pathway in tumor growth and angiogenesis. *J. Clin. Oncol.* **2005**, *23* (5), 1011−1027.

(11) Yang, C.; Guo, Y.; Jadlowiec, C. C.; Li, X.; Lv, W.; Model, L. S.; Collins, M. J.; Kondo, Y.; Muto, A.; Shu, C.; Dardik, A. Vascular endothelial growth factor-A inhibits EphB4 and stimulates delta-like ligand 4 expression in adult endothelial cells. *J. Surg. Res.* **2013**, *183* (1), 478−486.

(12) Li, D.; Liu, S.; Liu, R.; Park, R.; Hughes, L.; Krasnoperov, V.; Gill, P. S.; Li, Z.; Shan, H.; Conti, P. S. Targeting the EphB4 receptor for cancer diagnosis and therapy monitoring. *Mol. Pharmaceutics* **2013**, *10* (1), 329−336.

(13) Lafleur, K.; Huang, D.; Zhou, T.; Caflisch, A.; Nevado, C. Structure-based optimization of potent and selective inhibitors of the tyrosine kinase erythropoietin producing human hepatocellular carcinoma receptor B4 (EphB4). *J. Med. Chem.* **2009**, *52* (20), 6433−6446.

(14) Krasnoperov, V.; Kumar, S. R.; Ley, E.; Li, X.; Scehnet, J.; Liu, R.; Zozulya, S.; Gill, P. S. Novel EphB4 monoclonal antibodies modulate angiogenesis and inhibit tumor growth. *Am. J. Pathol.* **2010**, *176* (4), 2029−2038.

(15) Peters, K. G. Vascular Endothelial Growth Factor and the Angiopoietins. *Circ. Res.* **1998**, *83* (3), 342−343.

(16) Chen, D.; Hughes, E. D.; Saunders, T. L.; Wu, J.; Vasquez, M. N. H.; Makinen, T.; King, P. D. Angiogenesis depends upon EPHB4-mediated export of collagen IV from vascular endothelial cells. *JCI Insight* **2022**, *7* (4), No. e156928.

(17) Kim, I.; Ryu, Y. S.; Kwak, H. J.; Ahn, S. Y.; Oh, J. L.; Yancopoulos, G. D.; Gale, N. W.; Koh, G. Y. EphB ligand, ephrinB2, suppresses the VEGF- and angiopoietin 1-induced Ras/mitogen-activated protein kinase pathway in venous endothelial cells. *FASEB J.* **2002**, *16* (9), 1126−1128.

(18) Dai, S.; Zhou, Z.; Chen, Z.; Xu, G.; Chen, Y. Fibroblast Growth Factor Receptors (FGFRs): Structures and Small Molecule Inhibitors. *Cells* **2019**, *8* (6), No. 614, DOI: 10.3390/cells8060614.
(19) Krook, M. A.; Reeser, J. W.; Ernst, G.; Barker, H.; Wilberding, M.; Li, G.; Chen, H. Z.; Roychowdhury, S. Fibroblast growth factor receptors in cancer: genetic alterations, diagnostics, therapeutic targets and mechanisms of resistance. *Br. J. Cancer* **2021**, *124* (5), 880−892.
(20) Wang, L.; Liu, W. Q.; Broussy, S.; Han, B.; Fang, H. Recent advances of anti-angiogenic inhibitors targeting VEGF/VEGFR axis. *Front. Pharmacol.* **2023**, *14*, No. 1307860.
(21) Carmeliet, P.; Jain, R. K. Molecular mechanisms and clinical applications of angiogenesis. *Nature* **2011**, *473* (7347), 298−307.
(22) Yoo, S. Y.; Kwon, S. M. Angiogenesis and its therapeutic opportunities. *Mediators Inflammation* **2013**, *2013*, No. 127170.
(23) Schmieder, R.; Hoffmann, J.; Becker, M.; Bhargava, A.; Müller, T.; Kahmann, N.; Ellinghaus, P.; Adams, R.; Rosenthal, A.; Thierauch, K. H.; Scholz, A.; Wilhelm, S. M.; Zopf, D. Regorafenib (BAY 73−4506): antitumor and antimetastatic activities in preclinical models of colorectal cancer. *Int. J. Cancer* **2014**, *135* (6), 1487−1496.
(24) Sharma, S.; Johnson, D.; Abouammoh, M.; Hollands, S.; Brissette, A. Rate of serious adverse effects in a series of bevacizumab and ranibizumab injections. *Can. J. Ophthalmol.* **2012**, *47* (3), 275−279.
(25) Motzer, R. J.; Rini, B. I.; Bukowski, R. M.; Curti, B. D.; George, D. J.; Hudes, G. R.; Redman, B. G.; Margolin, K. A.; Merchan, J. R.; Wilding, G.; Ginsberg, M. S.; Bacik, J.; Kim, S. T.; Baum, C. M.; Michaelson, M. D. Sunitinib in patients with metastatic renal cell carcinoma. *JAMA* **2006**, *295* (21), 2516−2524.
(26) Hanahan, D.; Folkman, J. Patterns and emerging mechanisms of the angiogenic switch during tumorigenesis. *Cell* **1996**, *86* (3), 353−364.
(27) Abdel-Mohsen, H. T.; Ibrahim, M. A.; Nageeb, A. M.; El Kerdawy, A. M. Receptor-based pharmacophore modeling, molecular docking, synthesis and biological evaluation of novel VEGFR-2, FGFR-1, and BRAF multi-kinase inhibitors. *BMC Chem.* **2024**, *18* (1), No. 42.
(28) Zhang, Q.; Li, Z.; Zhang, J.; Li, Y.; Pan, X.; Qu, J.; Zhang, J. Novel multi-target angiogenesis inhibitors as potential anticancer agents: Design, synthesis and preliminary activity evaluation. *Bioorg. Chem.* **2024**, *145*, No. 107211.
(29) Azimian, F.; Dastmalchi, S. Recent Advances in Structural Modification Strategies for Lead Optimization of Tyrosine Kinase Inhibitors to Explore Novel Anticancer Agents. *Curr. Med. Chem.* **2023**, *30* (24), 2734−2761.
(30) Allam, R. M.; El Kerdawy, A. M.; Gouda, A. E.; Ahmed, K. A.; Abdel-Mohsen, H. T. Benzimidazole-oxindole hybrids as multi-kinase inhibitors targeting melanoma. *Bioorg. Chem.* **2024**, *146*, No. 107243.
(31) Akwata, D.; Kempen, A. L.; Dayal, N.; Brauer, N. R.; Sintim, H. O. Identification of a Selective FLT3 Inhibitor with Low Activity against VEGFR, FGFR, PDGFR, c-KIT, and RET Anti-Targets. *ChemMedChem* **2024**, *19* (1), No. e202300442.
(32) Ezelarab, H. A.; Abd El-Hafeez, A. A.; Ali, T. F.; Sayed, A. M.; Hassan, H. A.; Beshr, E. A.; Abbas, S. H. New 2-oxoindole derivatives as multiple PDGFRα/ß and VEGFR-2 tyrosine kinase inhibitors. *Bioorg. Chem.* **2024**, *145*, No. 107234.
(33) Li, C.-Q.; Lei, H.-M.; Hu, Q.-Y.; Li, G.-H.; Zhao, P.-J. Recent Advances in the Synthetic Biology of Natural Drugs. *Front. Bioeng. Biotechnol.* **2021**, *9*, No. 691152, DOI: 10.3389/fbioe.2021.691152.
(34) Dias, D. A.; Urban, S.; Roessner, U. A historical overview of natural products in drug discovery. *Metabolites* **2012**, *2* (2), 303−336.
(35) Atanasov, A. G.; Zotchev, S. B.; Dirsch, V. M.; Orhan, I. E.; Banach, M.; Rollinger, J. M.; Barreca, D.; Weckwerth, W.; Bauer, R.; Bayer, E. A.; Majeed, M.; Bishayee, A.; Bochkov, V.; Bonn, G. K.; Braidy, N.; Bucar, F.; Cifuentes, A.; D'Onofrio, G.; Bodkin, M.; Diederich, M.; Dinkova-Kostova, A. T.; Efferth, T.; El Bairi, K.; Arkells, N.; Fan, T.-P.; Fiebich, B. L.; Freissmuth, M.; Georgiev, M. I.; Gibbons, S.; Godfrey, K. M.; Gruber, C. W.; Heer, J.; Huber, L. A.; Ibanez, E.; Kijjoa, A.; Kiss, A. K.; Lu, A.; Macias, F. A.; Miller, M. J. S.; Mocan, A.; Müller, R.; Nicoletti, F.; Perry, G.; Pittalà, V.; Rastrelli, L.; Ristow, M.; Russo, G. L.; Silva, A. S.; Schuster, D.; Sheridan, H.; Skalicka-Woźniak, K.; Skaltsounis, L.; Sobarzo-Sánchez, E.; Bredt, D. S.; Stuppner, H.; Sureda, A.; Tzvetkov, N. T.; Vacca, R. A.; Aggarwal, B. B.; Battino, M.; Giampieri, F.; Wink, M.; Wolfender, J.-L.; Xiao, J.; Yeung, A. W. K.; Lizard, G.; Popp, M. A.; Heinrich, M.; Berindan-Neagoe, I.; Stadler, M.; Daglia, M.; Verpoorte, R.; Supuran, C. T.; the International Natural Product Sciences Taskforce. Natural products in drug discovery: advances and opportunities. *Nat. Rev. Drug Discovery* **2021**, *20* (3), 200−216.
(36) Beutler, J. A. Natural Products as a Foundation for Drug Discovery. *Curr. Protoc. Pharmaco.l* **2009**, *46*, 9.11.1−9.11.21.
(37) Dai, B.; Qi, J.; Liu, R.; Zhang, J.; Zhan, Y.; Zhang, Y. A novel compound T7 (N-{4′-[(1E)-N-hydroxyethanimidoyl]-3′,5,6-trimethoxybiphenyl-3-yl}-N′-[4-(3-morpholin-4-ylpropoxy)phenyl]urea) screened by tissue angiogenesis model and its activity evaluation on anti-angiogenesis. *Phytomedicine* **2014**, *21* (12), 1675−1683.
(38) Peng, Y. H.; Shiao, H. Y.; Tu, C. H.; Liu, P. M.; Hsu, J. T.; Amancha, P. K.; Wu, J. S.; Coumar, M. S.; Chen, C. H.; Wang, S. Y.; Lin, W. H.; Sun, H. Y.; Chao, Y. S.; Lyu, P. C.; Hsieh, H. P.; Wu, S. Y. Protein kinase inhibitor design by targeting the Asp-Phe-Gly (DFG) motif: the role of the DFG motif in the design of epidermal growth factor receptor inhibitors. *J. Med. Chem.* **2013**, *56* (10), 3889−3903.
(39) Vijayan, R. S. K.; He, P.; Modi, V.; Duong-Ly, K. C.; Ma, H.; Peterson, J. R.; Dunbrack, R. L., Jr.; Levy, R. M. Conformational analysis of the DFG-out kinase motif and biochemical profiling of structurally validated type II inhibitors. *J. Med. Chem.* **2015**, *58* (1), 466−479.
(40) Koch, M. A.; Schuffenhauer, A.; Scheck, M.; Wetzel, S.; Casaulta, M.; Odermatt, A.; Ertl, P.; Waldmann, H. Charting biologically relevant chemical space: A structural classification of natural products (SCONP). *Proc. Natl. Acad. Sci. U.S.A.* **2005**, *102* (48), 17272−17277.
(41) Tajabadi, F. M.; Pouwer, R. H.; Liu, M.; Dashti, Y.; Campitelli, M. R.; Murtaza, M.; Mellick, G. D.; Wood, S. A.; Jenkins, I. D.; Quinn, R. J. Design and Synthesis of Natural Product Inspired Libraries Based on the Three-Dimensional (3D) Cedrane Scaffold: Toward the Exploration of 3D Biological Space. *J. Med. Chem.* **2018**, *61* (15), 6609−6628.
(42) Marcaurelle, L. A.; Johannes, C. W. Application of natural product-inspired diversity-oriented synthesis to drug discovery. In *Natural Compounds as Drugs, Volume II*; Petersen, F.; Amstutz, R., Eds.; Birkhäuser Basel: Basel, 2008; pp 187−216.
(43) Gagare, S.; Patil, P.; Jain, A. Natural product-inspired strategies towards the discovery of novel bioactive molecules. *Future J. Pharm. Sci.* **2024**, *10* (1), No. 55.
(44) Rodrigues, T.; Reker, D.; Schneider, P.; Schneider, G. Counting on natural products for drug design. *Nat. Chem.* **2016**, *8* (6), 531−541.
(45) Ganesan, A. The impact of natural products upon modern drug discovery. *Curr. Opin. Chem. Biol.* **2008**, *12* (3), 306−317.
(46) Lee, M. L.; Schneider, G. Scaffold architecture and pharmacophoric properties of natural products and trade drugs: application in the design of natural product-based combinatorial libraries. *J. Comb. Chem.* **2001**, *3* (3), 284−289.
(47) van Hattum, H.; Waldmann, H. Biology-Oriented Synthesis: Harnessing the Power of Evolution. *J. Am. Chem. Soc.* **2014**, *136* (34), 11853−11859.
(48) Schaller, D.; Šribar, D.; Noonan, T.; Deng, L.; Nguyen, T. N.; Pach, S.; Machalz, D.; Bermudez, M.; Wolber, G. Next generation 3D pharmacophore modeling. *WIREs Comput. Mol. Sci.* **2020**, *10* (4), No. e1468.
(49) Jain, A. N. Virtual screening in lead discovery and optimization. *Curr. Opin. Drug Discovery Dev.* **2004**, *7* (4), 396−403.
(50) Shoichet, B. K. Virtual screening of chemical libraries. *Nature* **2004**, *432* (7019), 862−865.
(51) McTigue, M.; Murray, B. W.; Chen, J. H.; Deng, Y. L.; Solowiej, J.; Kania, R. S. Molecular conformations, interactions, and properties associated with drug efficiency and clinical performance

among VEGFR TK inhibitors. *Proc. Natl. Acad. Sci. U.S.A.* **2012**, *109* (45), 18281−18289.
(52) Tröster, A.; Heinzlmeir, S.; Berger, B. T.; Gande, S. L.; Saxena, K.; Sreeramulu, S.; Linhard, V.; Nasiri, A. H.; Bolte, M.; Müller, S.; Kuster, B.; Médard, G.; Kudlinzki, D.; Schwalbe, H. NVP-BHG712: Effects of Regioisomers on the Affinity and Selectivity toward the EPHrin Family. *ChemMedChem* **2018**, *13* (16), 1629−1633.
(53) Lin, Q.; Chen, X.; Qu, L.; Guo, M.; Wei, H.; Dai, S.; Jiang, L.; Chen, Y. Characterization of the cholangiocarcinoma drug pemigatinib against FGFR gatekeeper mutants. *Commun. Chem.* **2022**, *5* (1), No. 100.
(54) Harney, A. S.; Karagiannis, G. S.; Pignatelli, J.; Smith, B. D.; Kadioglu, E.; Wise, S. C.; Hood, M. M.; Kaufman, M. D.; Leary, C. B.; Lu, W. P.; Al-Ani, G.; Chen, X.; Entenberg, D.; Oktay, M. H.; Wang, Y.; Chun, L.; De Palma, M.; Jones, J. G.; Flynn, D. L.; Condeelis, J. S. The Selective Tie2 Inhibitor Rebastinib Blocks Recruitment and Function of Tie2(Hi) Macrophages in Breast Cancer and Pancreatic Neuroendocrine Tumors. *Mol. Cancer Ther.* **2017**, *16* (11), 2486−2501.
(55) Edgar, R. C. MUSCLE: multiple sequence alignment with high accuracy and high throughput. *Nucleic Acids Res.* **2004**, *32* (5), 1792−1797.
(56) Sorokina, M.; Merseburger, P.; Rajan, K.; Yirik, M. A.; Steinbeck, C. COCONUT online: Collection of Open Natural Products database. *J. Cheminf.* **2021**, *13* (1), No. 2.
(57) Rutz, A.; Sorokina, M.; Galgonek, J.; Mietchen, D.; Willighagen, E.; Gaudry, A.; Graham, J. G.; Stephan, R.; Page, R.; Vondrášek, J.; Steinbeck, C.; Pauli, G. F.; Wolfender, J.-L.; Bisson, J.; Allard, P.-M. The LOTUS initiative for open knowledge management in natural products research. *eLife* **2022**, *11*, No. e70780.
(58) Gallo, K.; Kemmler, E.; Goede, A.; Becker, F.; Dunkel, M.; Preissner, R.; Banerjee, P. SuperNatural 3.0—a database of natural products and natural product-based derivatives. *Nucleic Acids Res.* **2023**, *51* (D1), D654−D659.
(59) Baell, J. B.; Holloway, G. A. New Substructure Filters for Removal of Pan Assay Interference Compounds (PAINS) from Screening Libraries and for Their Exclusion in Bioassays. *J. Med. Chem.* **2010**, *53* (7), 2719−2740.
(60) Dixon, S. L.; Smondyrev, A. M.; Rao, S. N. PHASE: A Novel Approach to Pharmacophore Modeling and 3D Database Searching. *Chem. Biol. Drug Des.* **2006**, *67* (5), 370−372.
(61) Dixon, S. L.; Smondyrev, A. M.; Knoll, E. H.; Rao, S. N.; Shaw, D. E.; Friesner, R. A. PHASE: a new engine for pharmacophore perception, 3D QSAR model development, and 3D database screening: 1. Methodology and preliminary results. *J. Comput.-Aided Mol. Des.* **2006**, *20* (10), 647−671.
(62) Truchon, J.-F.; Bayly, C. I. Evaluating Virtual Screening Methods: Good and Bad Metrics for the "Early Recognition" Problem. *J. Chem. Inf. Model.* **2007**, *47* (2), 488−508.
(63) Lyne, P. D.; Lamb, M. L.; Saeh, J. C. Accurate prediction of the relative potencies of members of a series of kinase inhibitors using molecular docking and MM-GBSA scoring. *J. Med. Chem.* **2006**, *49* (16), 4805−4808.
(64) Gill, P. M. W.; Johnson, B. G.; Pople, J. A.; Frisch, M. J. The performance of the Becke—Lee—Yang—Parr (B—LYP) density functional theory with various basis sets. *Chem. Phys. Lett.* **1992**, *197* (4), 499−505.
(65) Madushanka, A.; Moura, R. T., Jr.; Verma, N.; Kraka, E. Quantum Mechanical Assessment of Protein-Ligand Hydrogen Bond Strength Patterns: Insights from Semiempirical Tight-Binding and Local Vibrational Mode Theory. *Int. J. Mol. Sci.* **2023**, *24* (7), No. 6311, DOI: 10.3390/ijms24076311.
(66) Clark, F.; Robb, G.; Cole, D. J.; Michel, J. Comparison of Receptor−Ligand Restraint Schemes for Alchemical Absolute Binding Free Energy Calculations. *J. Chem. Theory Comput.* **2023**, *19* (12), 3686−3704.
(67) Knegtel, R. M. A.; Grootenhuis, P. D. J.Binding affinities and non-bonded interaction energies. In *Perspectives in Drug Discovery and Design*; Springer, 1998; Vol. *9*, pp 99−114.
(68) Moradi, M.; Mousavi, A.; Emamgholipour, Z.; Giovannini, J.; Moghimi, S.; Peytam, F.; Honarmand, A.; Bach, S.; Foroumadi, A. Quinazoline-based VEGFR-2 inhibitors as potential anti-angiogenic agents: A contemporary perspective of SAR and molecular docking studies. *Eur. J. Med. Chem.* **2023**, *259*, No. 115626.
(69) Malekan, M.; Ebrahimzadeh, M. A. Vascular endothelial growth factor receptors [VEGFR] as target in breast cancer treatment: current status in preclinical and clinical studies and future directions. *Curr. Top. Med. Chem.* **2022**, *22* (11), 891−920.
(70) Oguro, Y.; Cary, D. R.; Miyamoto, N.; Tawada, M.; Iwata, H.; Miki, H.; Hori, A.; Imamura, S. Design, synthesis, and evaluation of novel VEGFR2 kinase inhibitors: discovery of [1, 2, 4] triazolo [1, 5-a] pyridine derivatives with slow dissociation kinetics. *Bioorg. Med. Chem.* **2013**, *21* (15), 4714−4729.
(71) Saleh, N. M.; Abdel-Rahman, A. A. H.; Omar, A. M.; Khalifa, M. M.; El-Adl, K. Pyridine-derived VEGFR-2 inhibitors: rational design, synthesis, anticancer evaluations, in silico ADMET profile, and molecular docking. *Arch. Pharm.* **2021**, *354* (8), No. 2100085.
(72) Kubo, K.; Shimizu, T.; Ohyama, S.-i.; Murooka, H.; Iwai, A.; Nakamura, K.; Hasegawa, K.; Kobayashi, Y.; Takahashi, N.; Takahashi, K.; et al. Novel potent orally active selective VEGFR-2 tyrosine kinase inhibitors: synthesis, structure− activity relationships, and antitumor activities of n-phenyl-n ′-{4-(4-quinolyloxy) phenyl} ureas. *J. Med. Chem.* **2005**, *48* (5), 1359−1366.
(73) Adel, M.; Abouzid, K. A. New fluorinated diarylureas linked to pyrrolo [2, 3-d] pyrimidine scaffold as VEGFR-2 inhibitors: Molecular docking and biological evaluation. *Bioorg. Chem.* **2022**, *127*, No. 106006.
(74) Wang, K.; Chen, Q.; Liu, N.; Zhang, J.; Pan, X. Recent advances in, and challenges of, anti-angiogenesis agents for tumor chemotherapy based on vascular normalization. *Drug Discovery Today* **2021**, *26* (11), 2743−2753.
(75) Sharma, P. S.; Sharma, R.; Tyagi, T. VEGF/VEGFR pathway inhibitors as anti-angiogenic agents: present and future. *Curr. Cancer Drug Targets* **2011**, *11* (5), 624−653.
(76) Schenone, S.; Bondavalli, F.; Botta, M. Antiangiogenic agents: an update on small molecule VEGFR inhibitors. *Curr. Med. Chem.* **2007**, *14* (23), 2495−2516.
(77) Nakamura, K.; Taguchi, E.; Miura, T.; Yamamoto, A.; Takahashi, K.; Bichat, F.; Guilbaud, N.; Hasegawa, K.; Kubo, K.; Fujiwara, Y.; et al. KRN951, a highly potent inhibitor of vascular endothelial growth factor receptor tyrosine kinases, has antitumor activities and affects functional vascular properties. *Cancer Res.* **2006**, *66* (18), 9134−9142.

https://doi.org/10.1021/acsomega.4c08366
ACS Omega 2025, 10, 13880−13897